POLITECNICO DI MILANO

Corso di Laurea in Ingengneria Aeronautica

Master Degree Thesis

Optimal design methods with choice of aerodynamic profiles for aircraft propellers

POLITECNICO
MILANO 1863

Relatore
Lorenzo Trainelli

Correlatore
Carlo E. D. Riboldi

Candidato
Jaime de Zubeldia Martín

A.A. 2019/2020

Contents

List of Figures

List of Tables

List of symbols

a_x	Axial interference factor
a_y	Rotational interference factor
AoA	Angle of attack
b_i	Bernstein i coefficient
B	Number of blades
B	Bézier curve value
BEMT	Blade Element Momentum Theory
c	Chord
C_D	Drag coefficient
C_L	Lift coefficient
C_T	Thrust coefficient
C_Q	Torque coefficient
C_X	X force coefficient
C_Y	Y force coefficient
D	Diameter
dT	Thrust per unit span
dQ	Torque per unit span
f	Prandtl-Glauert correction coefficient
F	Prandtl tip loss factor
H	Geometrical propeller pitch
J	Advance ratio
K	Goldstein momentum loss factor
lb	Lower boundary admitted for optimization variables
n	Number of stations
n_s	Rotations per second
N	Number of Bézier control points
M	Mach number
$\mathbf{P_i}$	Bézier control point i
t	Bézier parameter
T	Total Thrust
Q	Total torque
r	Axial distance from axis of rotation
$R_{\text{cut-off}}$	Cut-off radius
Re	Reynolds number
ub	Upper boundary admitted for optimization variables
V_X	Axial flow speed
V_Y	Radial flow speed
W	Local airspeed
β	Twist angle
γ	Parameter of Fobj
ϵ	Difference of W between iterations
η	Efficiency
η_{cruise}	Efficiency in cruise conditions
η_{max}	Maximum efficiency
θ	Blade pitch
ξ	Non dimensional radius
ρ	Density
σ	Blade solidity
ϕ	Inflow angle
ϕ_{new}	Inflow angle in new iteration
ϕ_t	Inflow angle at the tip
ω	Angular velocity

Chapter 1

Introduction

This thesis is devoted to the development of a tool that enables the user to obtain optimized propeller geometry for a propeller that is optimum for different kinds of purposes, for example, but not necessarily, maximum efficiency in cruise conditions. On the one hand, there exists similar software on the web that provide optimal geometries for these purposes. However, the main advantage of designing such a tool relies on the definition of custom cost functions, and the possibility of defining arbitrary blade geometries, making the code much more versatile than those programs.

Firstly, is mandatory to obtain the capability of calculating propeller performance for arbitrary designs. In order to do this, performance calculations are obtained throughout a model widely studied in the past. The model utilized is the Blade Element Momentum Theory, for which geometry is parametrized in terms of diameter, number of blades, distribution of stations along the blade, twist and chord distributions and airfoil of the section. Fluid properties of the stream are also introduced in this model along with propeller working operation. The equations presented in Chapter 2 require the preparation of a polar database that contains the aerodynamic coefficients of the airfoils used in propeller blade sections prior to the start of the calculations.

Following model definition, it is necessary to verify the reliability of the calculations performed. To do so, propeller performance studied by Xiang in [1] is compared with the results obtained coming from the present model. In this article, Xiang proposes another kind of model for propeller performance calculations and it is analysed with wind tunnel test data. Later in this thesis, in Section 2.3, data from that experiment are used to validate the BEMT model, used in this whole document.

Once the model is set up, a sensibility assessment on the impact of some parameters that define propeller geometry in the solution is carried out in Chapter 3. Said parameters are the number of stations and their distribution along blade span, with a comparison of different distribution laws and the first station location, which is dependent on the hub dimensions. This analysis is useful as it introduces the parameters that must be fixed prior to an optimization routine.

Finally, the whole potential of the model is obtained in Chapter 4 where the first steps of an optimization procedure are detailed. In this chapter, optimized propeller geometry is calculated for a 19-passenger commuter in which the rest of the parameters that define propeller geometry are used as variables of optimization.

Finally, in Chapter 5, conclusions on the work performed along with recommendations for future studies are described, Appendix A contains a pseudocode of the implemented tool while Appendix B, contains a sensibility study on one of the minimization routine parameters.

Chapter 2

Synthesis of a blade performance model for design

The calculation of propeller performance have been studied long. Glauert in [2], analyses the different equations that model the propeller. A particular theory is exploited in this document: The Blade Element Momentum Theory. This model joins unidimensional momentum theory, in which the airscrews are approximated to a very thin disc that exchanges energy with airflow, and blade element theory, that takes into account the number of blades and their shapes to calculate the balance of forces in the rotor. Equations 2.1 to 2.4 display the main equations of momentum theory, while 2.5 to 2.7 those of blade element.

$$dT = C_T \frac{1}{2} \rho V_x^2 dA \tag{2.1}$$

$$dQ = C_Q \frac{1}{2} \rho V_x^2 dA r \tag{2.2}$$

In these equations of momentum theory, in order to calculate the forces that appear, the airscrew disk is divided in annular shapes of infinitesimal radius dr. For these annuli, the area dA can be approximated to rdr. In this manner, dT and dQ correspond to thrust and torque obtained in each annulus, and, to obtain the global forces, they should be integrated. For each annulus, thrust and torque coefficients are associated, namely C_T and C_Q. These coefficients are directly proportional to the acceleration that the fluid is subjected to, when passing through disk. This acceleration is taken into account with the help of the definition of interference parameters, a_x, that represent the axial acceleration, and a_y, that is related to the imprint of rotational motion to the fluid. These parameters appear in equations 2.3 and 2.4 along with F, a parameter that accounts for energy losses because of vortexes that appear.

$$C_T = 4F a_x (1 + a_x) \tag{2.3}$$

$$C_Q = 4F a_y (1 + a_x) \frac{V_y}{V_x} \tag{2.4}$$

As it was mentioned, blade element theory uses airfoil polars, that in the tool developed are obtained as described in Section 2.1.3. In this case, it can be written:

$$dT = BC_x \frac{1}{2} \rho W^2 c dr \tag{2.5}$$

$$dQ = BC_y \frac{1}{2} \rho W^2 c r dr \tag{2.6}$$

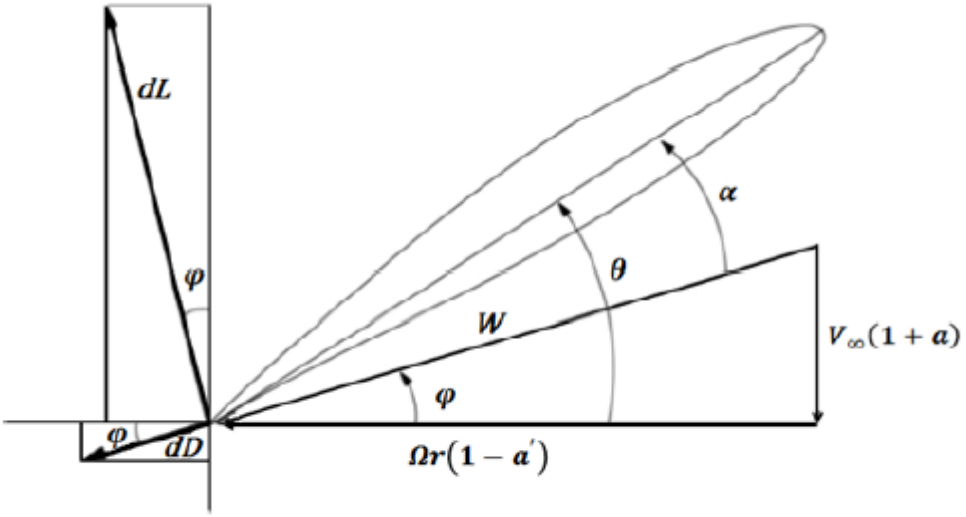

Figure 2.1: Forces in blade section [3]

Where again, the airscrew, now made up of blades, is divided radially in stations. For each station, the forces that appear in each of the blades must be taken into account. Therefore, in equations 2.5 and 2.6, B stands for the number of blades, C_T and C_Q have the same meaning, but are calculated differently as they are a function of the plan form of the blade section, c is the chord of the airfoil at the station and with $W = \sqrt{((V_x(1+a_x))^2 + (V_y(1-a_y))^2}$, being W the module of the airflow speed, but in this case:

$$\begin{bmatrix} C_x \\ C_y \end{bmatrix} = \begin{bmatrix} \cos\phi & -\sin\phi \\ \sin\phi & \cos\phi \end{bmatrix} \begin{bmatrix} C_l \\ C_d \end{bmatrix} \tag{2.7}$$

With C_l, C_d, being lift and drag coefficients and C_x, C_y, being force coefficients in axial and tangential directions respectively. By making equal the quantities dT and dQ obtained from the different theories, these equations lead to the following coupled solution, where ϕ is the inflow angle (or the difference between local β and α), angle that fixes the direction of local airstream:

$$a_x = \frac{C_x \sigma}{4F\sin^2\phi - C_x\sigma} \tag{2.8}$$

$$a_y = \frac{C_y \sigma}{2F\sin 2\phi + C_y\sigma} \tag{2.9}$$

Knowing the value of the interference parameters, the rest of the parameters involved in past equations can be obtained. This model is used to obtain propeller performance and, to solve the past equations, an assessment is carried out in Section 2.2, where the methods proposed by Adkins [4] and by Ning [5] are compared.

Once BEMT equations are solved, and the quantities C_x and C_y are known, thrust and torque per station are computed through equations 2.5 and 2.6. Then, total thrust and torque are obtained, summing the contributions of each section in which the blade is divided in, through a trapezoidal approximation, where the subindexes i and i+1 correspond to their corresponding stations, and r is the station axial position:

$$T = \sum_{i=1}^{n-1} \frac{dT_i + dT_{i+1}}{2} r_{i+1} - r_i \tag{2.10}$$

$$Q = \sum_{i=1}^{n-1} \frac{dQ_i + dQ_{i+1}}{2} r_{i+1} - r_i \tag{2.11}$$

Special attention must be paid at this point to how the spatial distribution is defined, since different distributions lead to different length of sections. An assessment on the effect of these distributions on the results is carried out in Section 3.1. Propeller efficiency is defined as, the coefficient between useful power, thrust force (T) by aircraft speed (V), and power required: torque needed (Q) at rotational speed of the engine (Ω). The choice of this definition is not arbitrary. In case of helicopters, where a hover flight condition is possible, this definition should be changed and written after a different figure of merit, since in hover, the airspeed far from the disk is zero, and, therefore, the efficiency would be null too.

$$\eta = \frac{TV}{\Omega Q} \tag{2.12}$$

Other non dimensional quantities that help compare propeller performance are now defined in equations from 2.13 to 2.16:

$$J = \frac{V}{n_s D} \tag{2.13}$$

$$C_T = \frac{T}{\rho n_s^2 D^4} \tag{2.14}$$

$$C_Q = \frac{Q}{\rho n_s^2 D^5} \tag{2.15}$$

$$C_P = \frac{Q}{\rho n_s^3 D^5} \tag{2.16}$$

Parameter J is called advance ratio and is used when operating conditions of a propeller are defined, so that propeller performance C_T and C_Q C_P and η, can be recalled.

2.1 Model implementation

The tool developed in this thesis implements the set of equations presented at the beginning of this chapter. In order to solve these equations, it is necessary to provide the tool the different parameters that affect propeller performance, and that are present in said equations. These parameters are geometrical, related to air flow conditions, and aerodynamic; and are explained in the following sections: Section 2.1.1, Section 2.1.2 and Section 2.1.3, respectively.

2.1.1 Geometry

A systematic approach to geometry definition is of paramount importance when developing a tool that is oriented to propeller design, especially because geometry characterization is one of the goals of this tool. A list of the parameters that must be determined is here presented.

- Number of blades (B)
- Diameter (D)
- Cut-off ratio ($R_{\text{Cut-off}}$)
- Distribution of stations along the blade (ξ(r))
- Chord and twist distributions (c(ξ(r)) and $\beta(\xi(r))$)

and also, another important parameter that have an impact on propeller geometry is:

- Number of stations (n)

Number of blades, diameter and cut-off are scalar magnitudes and do not present difficulties to be defined. On the other hand, twist and chord distributions require more attention: They can be figured out as curves that are a function of the distance from the axis of rotation, and therefore, there must be an adequate correlation between their definition and the distribution of stations along blade span.

Distribution of stations along the blade, twist and chord distributions are then carefully implemented as vectors, taking care that each position of twist and chord values are correctly assigned. Related to this, is the number of stations, a parameter that takes an important role in the quality of the results. The effect on the results of spatial resolution (in terms of number of stations) and the distribution of blades along the span is assessed in Section 3.1.

All past parameters are enough to describe propeller geometry. However, other parameters can be derived from them that take an active part in the BEMT equations, such as blade solidity, present in equations 2.27 and 2.28 and defined as the ratio of the total blade area to that of the circular disc swept by the blades.

$$\sigma = \frac{Bc}{2\pi r} \tag{2.17}$$

.

There also exist other aspects that can help comparing propellers of different geometries, like the geometrical pitch. Twist distribution of a propeller, namely, the set of angles of the sections with respect to the plane of rotation, determine the pitch of the airscrew. If the motion of the airscrew were that of a screw in a rigid medium, each section would advance

a distance $2\pi r \tan\beta$. This distance, H, is called the geometrical pitch of the propeller. A propeller of which its twist distribution follows the law present in equation 2.18, is said to have constant geometric pitch. For propellers that do not follow this twist distribution, their geometrical pitch is defined with the twist angle of a section, typically at 70% of the blade span. Geometrical pitch H, has no aerodynamic significance. However, the ratio of H/D is a useful measure to classify propellers. In fact, Figure 2.2 display the efficiency vs. advance ratio curves for a family of propellers for different values of H/D ratio.

$$\tan\beta = \frac{H}{2\pi r} \tag{2.18}$$

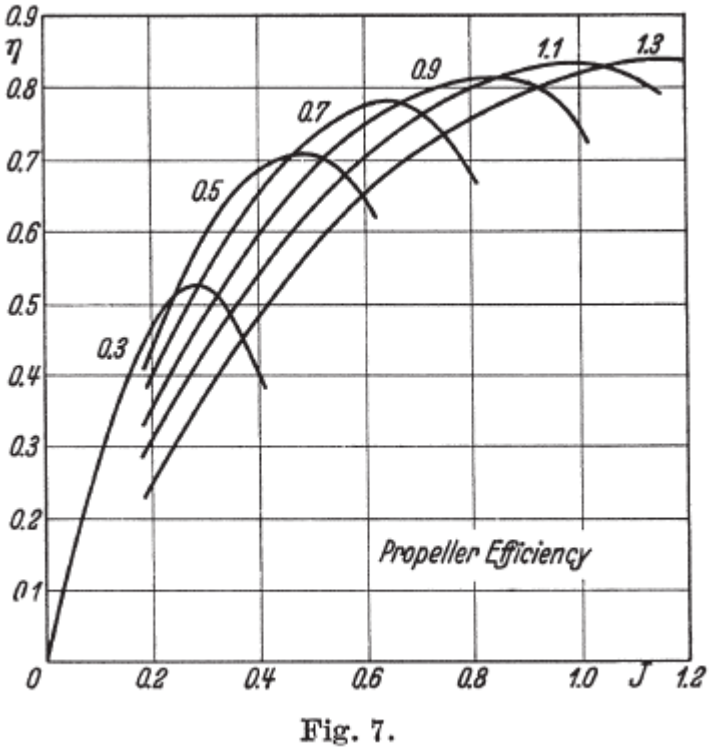

Fig. 7.

Figure 2.2: Efficiencies of a propeller family [2]

2.1.2 Air conditions

Propeller performance depends naturally on the fluid properties it is working in. The main important parameters are the following:

- Forward speed of the aircraft (V)
- Rotational speed (Ω or RPM)
- Density (ρ)
- Speed of sound (V_s)

Forward speed and rotational speed are summed to compute the module of the local flow speed, as in Figure 2.1. The tool works with the module of these speeds and are of easy implementation as they are scalar parameters. Density and temperature that are depend on the phase of the aircraft mission are needed to compute Reynolds and Mach numbers, numbers that lift and drag coefficients are function of.

2.1.3 Aerodynamics

The whole description of the blade element of BEMT reflects the necessity of knowing, at some point of the calculations, lift and drag coefficients of the section. These are a function of Reynolds and Mach numbers; section angle of attack; and of course, airfoil of the section. Two main issues arise when trying to write a code that solve the BEMT equations, which are: how to obtain airfoil characteristics and when does the routine need them. Starting by the latter, it is clear that, the process of solving BEMT equations affects the times in which the user needs to provide lift an drag coefficients as an input, and depending on the routine, this number of times varies, as in Section 2.2 in which two different procedures are presented.

The characterization of lift and drag coefficients of wings with different airfoils have been studied long, and many methods that provide approximations exist. A possible solution for the problem of providing lift and drag coefficients could be calculating them directly by an implementation of any existing method. On the other hand, it is possible to call other routines that calculate aerodynamic coefficients only when it is needed to. XFOIL is an interactive program for the design and analysis of subsonic isolated airfoils [6]. Developed by professor Mark Drela and released under the GNU General Public License,can be used to obtain the aerodynamic information searched. Therefore it is possible to call XFOIL during the resolution of the BEMT equations, or write a program that automatizes the creation of a database of polar curves for different Reynolds and Mach numbers. This database is created prior to the start of the calculations and retrieved during program execution.

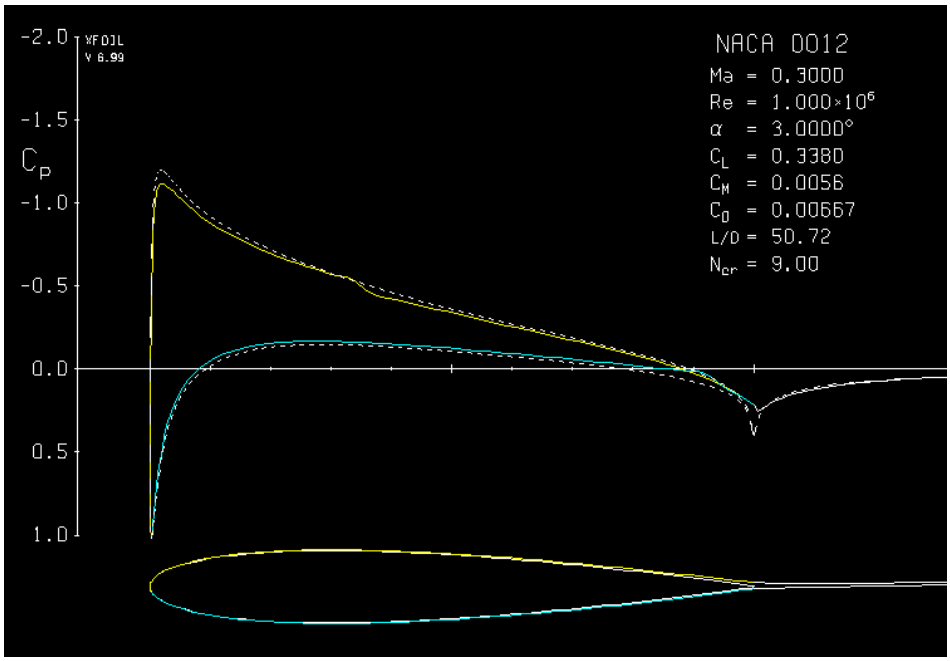

Figure 2.3: XFOIL environment

Calling XFOIL between iterations in order to obtain directly lift and drag coefficients is very flexible, and, in the case it was necessary, could allow a parametrization of airfoil geometry in order to include this parametrization as a variable during propeller geometry optimization. However, this would be very time consuming. In fact, in [3], Tarraran carries out an assessment on what is better in terms of computational time, and creating a database of polars reduces it drastically. This database of polars is unique for each airfoil, and therefore, said parametrization could not be considered, since airfoil shape between iterations is not known until the optimization routine starts.

Preparing a polar database presents new difficulties itself. XFOIL is designed to provide subsonic data and, for high subsonic Mach numbers, it is inaccurate, therefore, other sources of aerodynamic data must be considered in order to compensate the absence this data. In fact, for the optimizations performed in Chapter 4, it was necessary to consult other references, and to extrapolate data for angles of attack higher than that of stall with Viterna method [7] that is explained in Paragraph 2.1.3. In [8], data for the NACA 0012 symmetric airfoil at high subsonic Mach numbers, gathered from wind tunnel experiments, is provided. An example of this data is displayed in Figure 2.4.

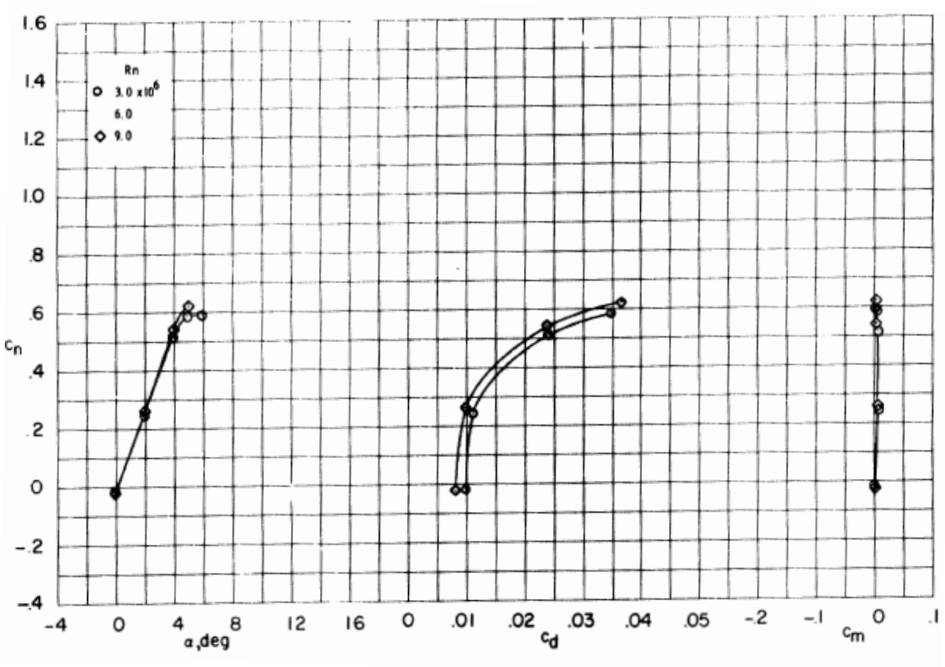

Figure 2.4: C_L and C_D of NACA 0012 M = 0.74 [8]

The database is therefore, created in XFOIL. This program allows to export the calculations as text files that saved into a folder an lately, opened by other computer programs. Thus, once the text files are created, the database should be ready. This is what Tarraran did in [3]. At this point, other text files containing polars can be created from other sources and included in the database. Finally, it is highly recommended to prepare a routine that reads every text file present in the database folder so all the data can be stowed in a variable in the environment in which the model is implemented, following the flow displayed in Figure 2.5, so that it is not necessary to open and close text files, but to read a local variable. The main drawback of loading the database directly in this manner is that it is required that the computer saves memory for this variable, however, the computational time is highly reduced thanks to this.

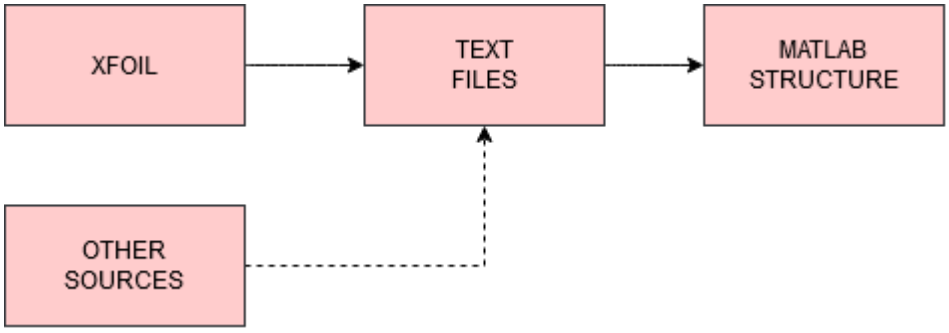

Figure 2.5: Polar database preparation flow

Text files that form the polar database are composed of columns of data of lift and drag coefficients as a function of angle of attack. Every text file contains these values for a couple of Reynolds and Mach values. For every airfoil used during the work of this thesis, the Reynolds and Mach numbers of which the database is made of, take discrete values from $5\,10^4$ up to $5\,10^6$ in steps of $5\,10^4$ in the case of Reynolds number and 0 up to 0.5 in steps of 0.05. Every time it is wanted to consult the database, it is necessary to perform an interpolation between the files that contain the closest Reynolds and Mach numbers available.

Viterna extrapolation

In order to be as robust as possible, the tool must be able to provide propeller performance in conditions in which not only some of the stations are subjected to local post-stall angles of attack, but also when the whole blade is stalled. This situation can appear for several reasons: low horizontal speed versus rotational speed ratio, high pitch of the blade, etcetera. It is necessary to extrapolate the data of aerodynamic coefficients for post stall angles so that it is possible to obtain lift an drag coefficients, regardless local angle of attack, within optimization routines, like in Chapter 4.

Viterna extrapolation is performed according to the equations of [7], compared with other methods in [9]. This method takes into account stall angle of attack and lift coefficient, maximum drag coefficient and aspect ratio of the blade to provide this extrapolation with the following equations:

$$C_D = B_1 \sin^2\alpha + B_2 \cos^2\alpha \tag{2.19}$$

$$C_L = A_1 \sin 2\alpha + A_2 \frac{\cos^2\alpha}{\sin\alpha}; \tag{2.20}$$

Being C_L and C_D the lift and drag coefficients that are wanted to approximate. The whole behaviour of the polar must be known prior to doing this approximation, as lift and drag coefficients at stall angle of attack (C_{L_s}, C_{D_s} and α_s) must be provided along with maximum drag (C_{D_m}). In this case, A_1, A_2, B_1, B_2 are defined and are proportional to said quantities:

$$A_1 = B_1/2; \tag{2.21}$$

$$A_2 = (C_{L_s} - C_{D_m} \sin\alpha_s \cos\alpha_s)\frac{\sin\alpha_s}{\cos^2\alpha_s}; \tag{2.22}$$

$$B_1 = C_{D_m} \tag{2.23}$$

$$B_2 = (C_{D_s} - C_{D_m}) \frac{\sin^2 \alpha_s}{\cos \alpha_s}; \tag{2.24}$$

2.2 Robustness assessment

How the BEMT equations are solved can lead to problems depending on the method used. In fact, Tarraran used in his final master degree thesis [3], an iterative method proposed by Adkins in [4]. This article contains two iterative algorithms: one for optimum propeller design, in which geometry of the design point is retrieved for when minimum energy loss conditions are met; and another that enables the calculation of propeller performance for arbitrary designs. Figure 2.6 displays the latter.

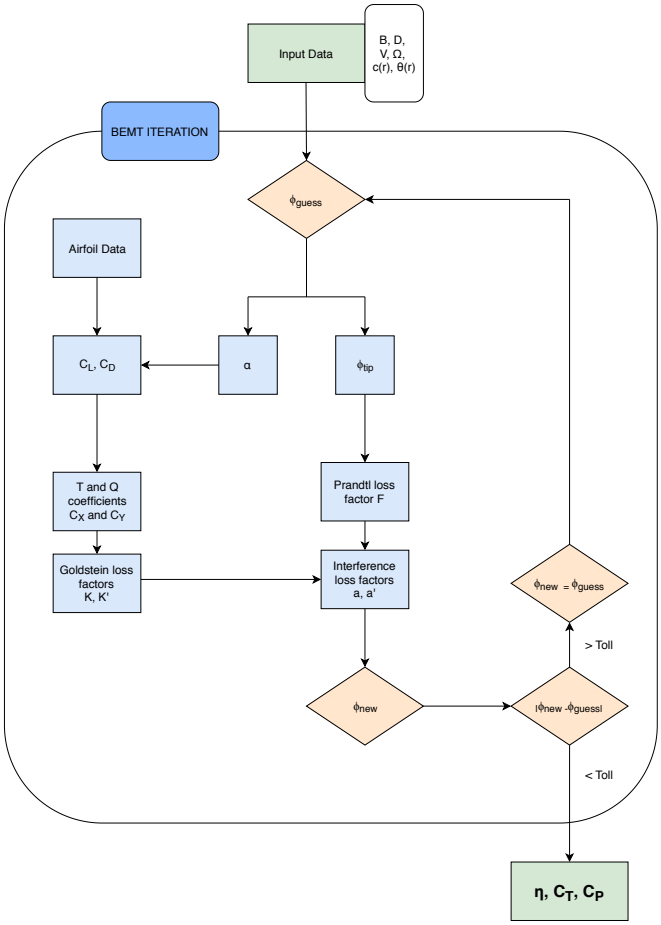

Figure 2.6: BEMT equations calculation algorithm [4]

Starting with known chord and twist distributions, number of blades, airfoil of the section and diameter of the propeller, an initial guess is used for ϕ. Figure 2.1 displays the relationship between inflow angle, angle of attack and local twist angle. Knowing this relationship, angle

of attack is obtained with the initial guess and the known twist distribution. Angle of attack, Reynolds and Mach numbers make it possible to compute the lift and drag coefficients. C_x and C_y are later computed through 2.7 and the process continues by calculating Goldstein loss factors K and K' as:

$$K = \frac{C_y}{4\sin^2\phi} \tag{2.25}$$

and

$$K' = \frac{C_x}{4\cos\phi\sin\phi} \tag{2.26}$$

Being these factors two parameters that account for losses and help the manipulation of BEMT equations for finding the searched solution. Thank to these, it is possible to calculate the interference factors, a_x and a_y as:

$$a_x = \frac{\sigma K}{F - \sigma K} \tag{2.27}$$

$$a_y = \frac{\sigma K'}{F + \sigma K'} \tag{2.28}$$

Prantl factor F for tip losses is calculated after the following expression taken from [4] (where π is the number π):

$$F = \frac{2}{\pi}\arccos e^{-f} \tag{2.29}$$

and where f is defined as in the following, being ϕ_t the value of the inflow angle at the tip.

$$f = \frac{B}{2}(1-\xi)/\sin\phi_t \tag{2.30}$$

Since BEMT equations are solved independently for each station, the calculations of inflow angle at the tip follow the condition of vortex sheet in the wake is a rigid screw surface, and this is obtained through the following equation:

$$\tan\phi_t = \xi\tan\phi \tag{2.31}$$

Finally, knowing the updated interference factors, recalling the triangle of speeds conformed by the axial (V) and rotational speeds (Ω) modified by the interference factors of Figure 2.1, the new direction of local airstream provides a new value of inflow angle, which is obtained through the following equation:

$$\phi_{new} = \arctan\frac{V(1+a_x)}{r\Omega(1-a_y)} \tag{2.32}$$

This new angle ϕ is compared with the value corresponding to current iteration value. If the difference is higher than the error admitted, the inflow angle value is updated and the algorithm restarts until ϕ converges. At this point, all the variables are already calculated and it is possible to obtain the propeller performance as detailed in Section 2.1. This algorithm may stop before arriving to convergence, as the calculations are sensitive once the Prandtl loss factor is calculated (eq. 2.29).

Even though past method is adequate for solving BEMT equations, the tool developed implements the solution found by Ning in [5], in which it is demonstrated that it is always possible to find a solution for equation 2.33. This equation is only function of the inflow

angle ϕ. Having fixed propeller geometry (σ), for given flight conditions of horizontal speed (V_x) and rotational speed (V_y at the station), and of course, having prepared a database of polars as provided in Section 2.1.3, it is only necessary to find the ϕ value that is solution of this equation.

$$V_y(4F\sin^2\phi - C_x\sigma) - V_x(2F\sin 2\phi + C_y\sigma) = 0 \tag{2.33}$$

Using Ning's approach to resolve BEMT equations the performance of a propeller that helped as an example in [4] was obtained. Adkins provides an example of the use of the algorithm described in its article and displayed in 2.6 for arbitrary design propeller performance. The propeller was designed to work at 110 mph (49m/s) and 2400 rpm. The airfoil of the section is the NACA 4415 and is maintained constant along the span. An extract of the article in which the geometry is defined is present in Table 2.1.

Table 2.1: Adkins' propeller example geometry definition [4]

r [mm]	c [mm]	β [deg]	ϕ [deg]
152.4	104.3	58.3	54.8
273.0	140.3	41.8	38.3
393.7	130.1	32.2	28.7
514.3	108.7	22.2	22.7
634.9	85.2	18.7	18.7
755.6	58.3	15.9	15.9
876.3	0.0	13.8	13.3

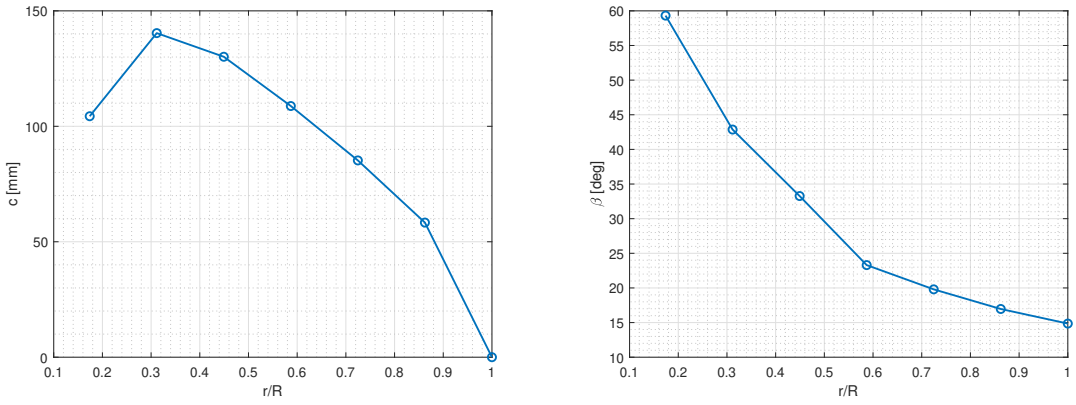

(a) *Chord distribution* (b) *Twist distribution*

Figure 2.7: Adkins propeller geometry

For this propeller, its performance was calculated and confronted with the results achieved in the article. Figures 2.8(c), 2.8(a) and 2.8(b) display two curves. Those in blue are obtained with the tool developed and in orange is the data present in the article, while an asterisk marks the design point for which the propeller was designed. Figure 2.8(d) does not provide information about the required torque coefficient obtained through Adkins algorithm as it there was no data provided.

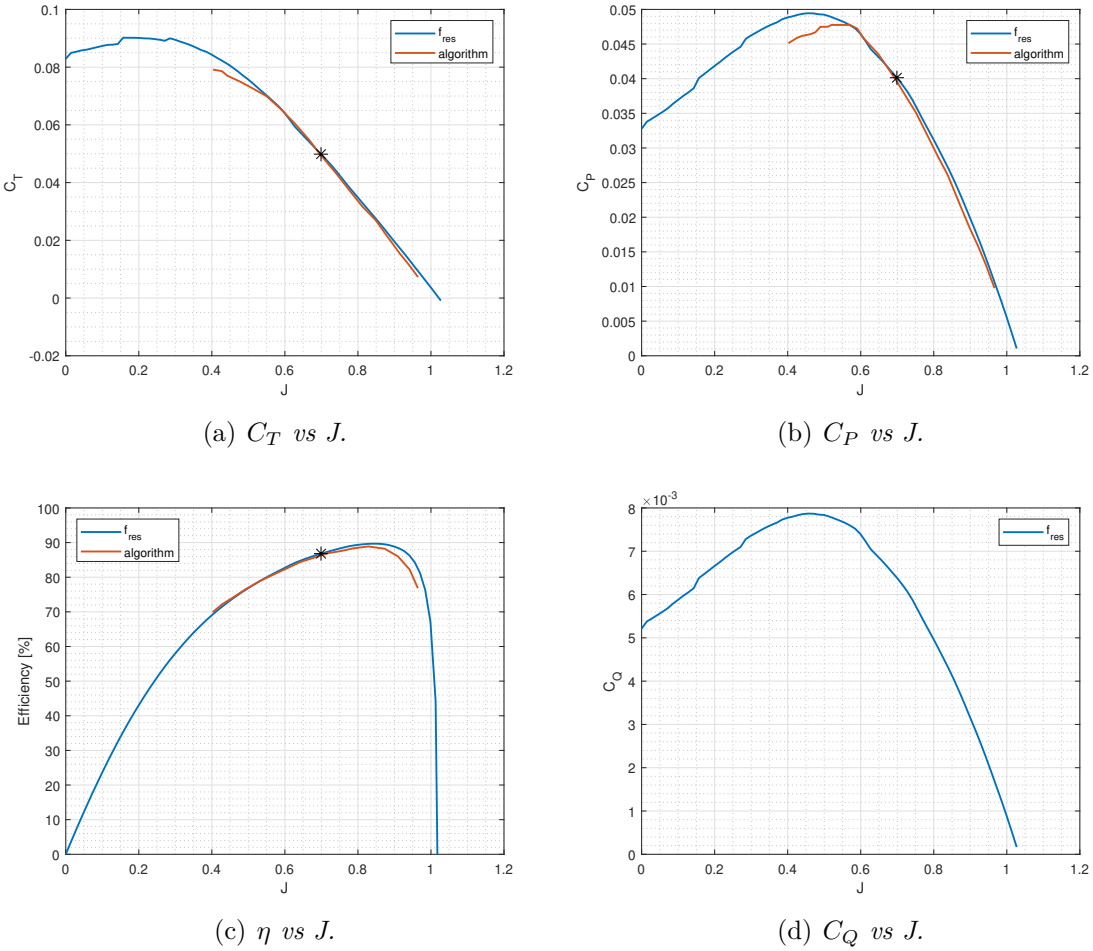

(a) C_T *vs* J.

(b) C_P *vs* J.

(c) η *vs* J.

(d) C_Q *vs* J.

Figure 2.8: Adkins propeller performance

The method proposed by Ning and the one by Adkins present a good agreement in the calculations. In fact, both procedures solve the same equations in a different manner.

Figures 2.8(a) and 2.8(b) display a slight deviation at values close to J = 0.45. In fact, there is no data available for J < 0.4 in the article. Recalling Section 2.1.3 in which the approximation of the aerodynamic coefficients for post-stall angles of attack is described, at J = 0.4, three out of the seven stations in which the blade is divided in are subjected to post stall angles of attack. This means that, for that small interval of advance ratio at which Adkins' data starts, different aerodynamic coefficients are used during the solving of propeller performance, and the approximating method utilized provides a small discrepancy in the results. It is thought that, if Adkins' data started at lower advance ratios, this difference would increase.

On the other hand, for higher advance ratios, very small deviations in the calculations performed are observed, being in accordance to what was said in the precedent paragraph. For higher advance ratios, there is no need for an approximation since sections are subjected to smaller angles of attack. These deviations may be due to the fact that Adkins' procedure of solving relies in the algorithm of Figure 2.6, and different choice of tolerances in the definition of convergence could be the cause of said deviations.

Overall, there is a good correlation between the computations of the two calculating

methods presented in this section.

2.3 Validation

The method proposed by Ning and adopted in the development of the tool, showed a good agreement with the method proposed by Adkins for calculating propeller performance. This concordance is promising, since in the article [4], the validity of the algorithm is positively checked by confronting calculations with real propeller performance data coming from experiments. Since the algorithm seems to provide results that are in accordance with tested data, and being the calculations performed by the tool here developed similar to those of the algorithm, it is possible to say that the tool provides reliable data. However, it has been decided to perform another confrontation with real propeller performance data more.

In the article of S.Xiang et al. [1], another method in for optimum propeller design is proposed and confronted with real data. The method is based on the article of optimum propeller design of Angelo et al. described in [10]. This is different to that of the previous section in the calculations of propeller performance. In fact, an algorithm for optimum propeller design there provided consists in a minimization of the condition of Glauert for energy losses by exploiting the use of Lagrange multipliers.

Similarly like in [4], the authors compared the results of their proposed method with data coming from wind tunnel tests of a scaled version of a propeller designed by their method in Northwestern Polytechnical University, China. The dimensions of the wind tunnel of rectangular section are 3.5m width, 2.5m height and 12m length. Turbulivity during the test was of 0.078%.

It is a two bladed propeller whose geometry is provided in Figure 2.9. Eight stations define chord and twist distributions. The airfoil used is the RAF 6 and is maintained constant along blade span. The diameter of the original propeller is 1.6 meters while the scaled version holds 0.96 meters of diameter. Figure 2.9 displaying propeller geometry has been taken directly from [1] and figures 2.9(a) and 2.9(b) display a linear behaviour of chord and twist distributions between stations rather than a smooth curve for both cases.

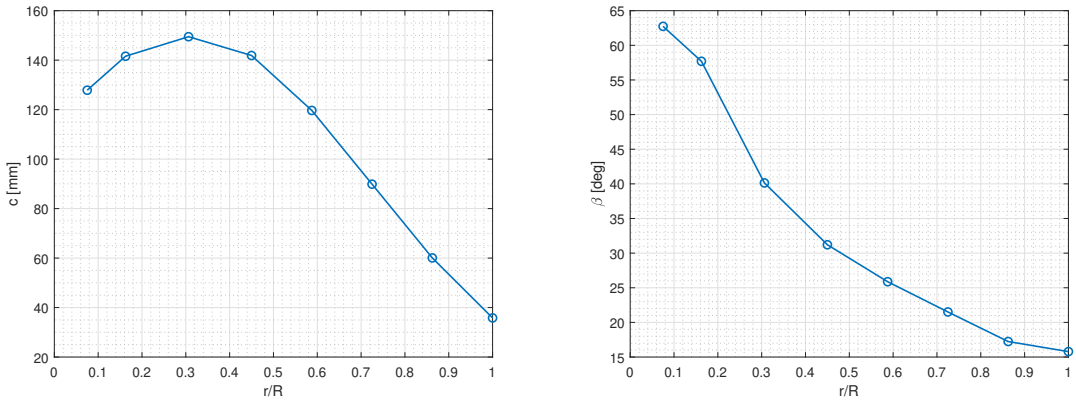

(a) *Chord distribution* (b) *Twist distribution*

Figure 2.9: Xiang propeller geometry

Figure 2.10 display the comparison between results obtained with the tool developed in blue, the calculations obtained with the method proposed by Xiang in orange and the data

coming from wind tunnel tests in yellow. Starting by the results obtained in [1], the trends of tunnel tests and Xiangs's method are in good accordance, however, a slight offset is present in 2.10(c). The results obtained with the tool developed in this thesis show a better agreement with data coming of wind tunnel tests rather than with the calculations performed following Xiang's method.

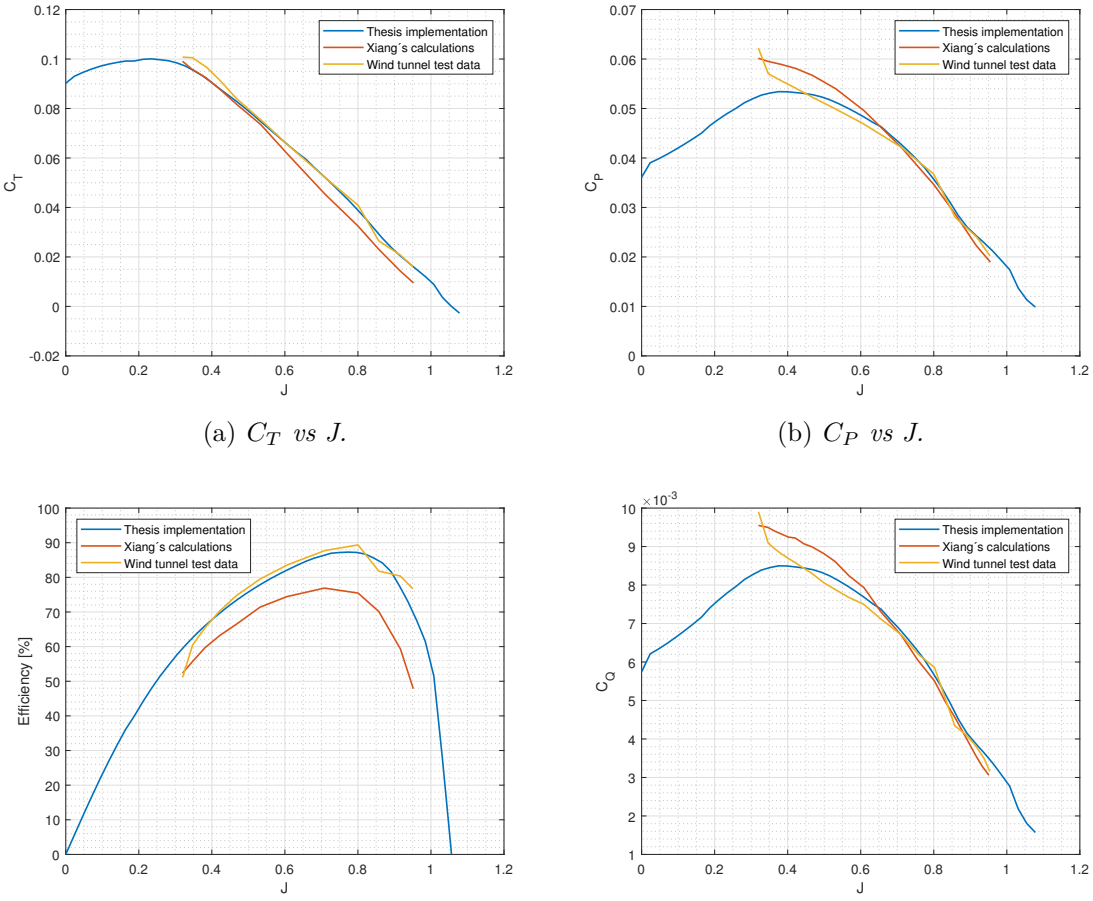

(a) C_T *vs* J.

(b) C_P *vs* J.

(c) η *vs* J.

(d) C_Q *vs* J.

Figure 2.10: Xiang propeller performance

In Xiang's article, the aerodynamic coefficients needed during the calculations are obtained in the same manner as in this thesis, throughout XFOIL. Therefore, it is thought that the discrepancies between the curves in blue of Figure 2.10 corresponding to the calculations performed in this thesis and the curves in orange, those of the calculations performed in Xiang's article, must be caused because of the different methods used. These differences are especially remarkable in the case of efficiency, in Figure 2.10(c).

On the other hand, the purpose of this analysis was to compare the calculations with experiment data, so that the discrepancies between propeller performance calculating methods is not that relevant. Comparing the blue curves with the yellow ones, a better agreement can be found. Again, like in Adkins' article, not data in the whole spectrum of J can be found in Xiang's document. It is noticeable that discrepancies occur at low J values, while a better accordance is found at higher advance ratio values. One of the reasons could be the small number of stations in which the blade was divided in to perform this assessment, since,

as described in future Section 3.1, for less than ten stations with uniform distribution, high errors can be encountered.

Chapter 3

Numerical studies

In this chapter the influence of number of stations, along with the spatial distribution of those and the influence of where the first station is placed is addressed. In these studies, the same propeller is analysed, whose characteristics are described in Table 3.1:

Table 3.1: Propeller geometry of Chapter 3 studies

Common	Section 3.1	Section 3.2
2 blades Diameter 1.75m NACA 4415 airfoil 900 RPM. $\rho = 1.225$ km/m^3 V sound = 343 m/s	20% $\xi_{\text{cut-off}}$ n variable	60 stations $\xi_{\text{cut-off}}$ variable

The geometry of this propeller is displayed in figures 3.1(a) and 3.1(b). Chord has been chosen to be 100 mm and constant along the span. Twist is defined with the following equation, equation 3.1:

$$\tan\beta = \frac{1.3D}{2\pi\xi} \tag{3.1}$$

This equation is similar to 2.18 in the Subsection 2.1.1, and it corresponds to a propeller of 1.3 H/D ratio. Looking at Figure 2.2, it is expected that the maximum efficiency of this propeller is in the advance ratio interval of [1:1.2], (which in fact it is, looking at 3.6). The benefits of using this formulation for the definition of twist distribution is that, once the distribution of stations has been defined, the calculations of twist distribution is straightforward, as a simple substitution in the past formula is enough.

Results of the following Sections show that efficiency is a parameter that is not much sensitive to the variations of the number of stations and $\xi_{\text{cut-off}}$, while torque and thrust are.

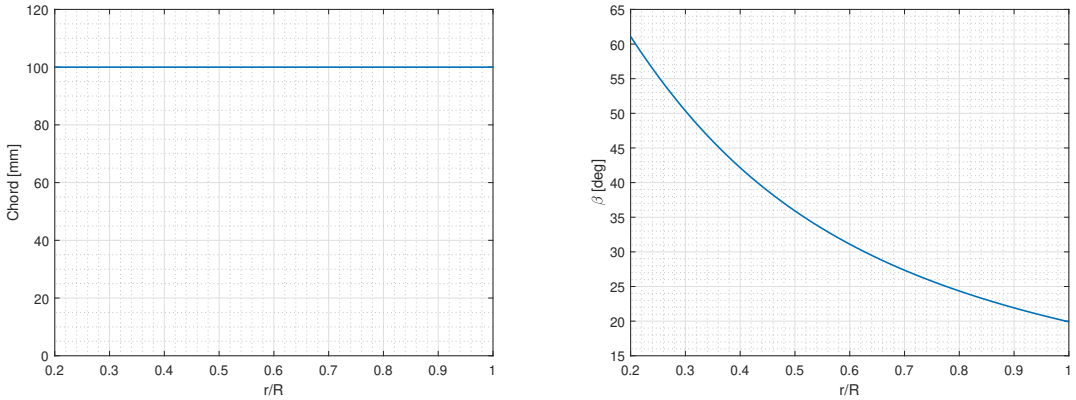

(a) *Chord distribution* (b) *Twist distribution*

Figure 3.1: Assessment propeller geometry

3.1 Spatial resolution assessment

As it has been said so, BEMT equations are solved individually for each station in which the blade is divided in, and each solution is not dependent on the other stations. In this section, an assessment of which spatial distribution of stations along blade span is better in terms of the quality of the result obtained is carried out. Two different distributions have been considered: a distribution that places stations uniformly along the blade span and a distribution that follows a cosine law that provides higher density near to the blade tip.

A good understanding about the effect of number of stations and how are they placed along the blade span is of paramount importance, since a small number of stations leads to errors in the calculations since geometry is poorly defined, and thrust and torque integration are directly dependent on this definition; however, high number of stations leads to higher computational time, an important quality aspect of the tool.

Figure 3.2 and equation 3.2 show how the distribution of stations with higher density near the blade tip is obtained. In a circumference of unitary radius, the angle value of which its cosine provides the desired position by the user of the first station is computed. Then, this angle is divided in n-1 equal parts, corresponding to n-1 sections of which the blade span is divided in, and their cosines are computed. It is trivial to remark that following this procedure, station values lie in the interval [$\xi_{\text{cut-off}}$, 1].

$$\xi_i = \cos\left(\left(1 - \frac{i-1}{n-1}\right)\arccos\xi_{cut-off}\right), \quad i = 1, 2, ..., n \tag{3.2}$$

The case for uniform distribution of stations follows equation 3.3. In this case, the density of stations along the blade span is uniform and the length of each of the sections obtained is constant.

$$\xi_i = \xi_{cut-off}\frac{n-i}{n-1} + \frac{i-1}{n-1}, \quad i = 1, 2, ..., n \tag{3.3}$$

Propellers analysed in Section 2.2 and Section 2.3, that of [4] and [1] respectively, have a limited number of stations as it can be seen in figures 2.7 and 2.9. In fact, only seven and eight stations were used in those references to calculate propeller performance. For this assessment. Performance the propeller whose geometry is displayed in Figure 3.1, has been

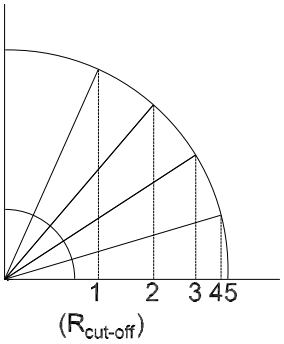

Figure 3.2: Representation of cosine distribution

calculated repeatedly for several increasing values of number of stations and a comparison is performed in figures 3.3(c), 3.3(b) and 3.3(a).

Firstly, the blade is divided into n stations, according to the formulations described before in equations 3.2 and 3.3. Then, chord and twist values are assigned properly to each station. Once blade geometry has been computed, aerodynamics and flight conditions are applied.

In Figure 3.3 the vertical axis represents the percentage of the difference between the calculated parameter with n number of stations and the same parameter but calculated with 150 stations with respect to the number of 150 stations like in equation 3.4, where P stands for the value of any kind of result that is wanted to be analysed: thrust, torque or efficiency. This equation allows the user to define a threshold of admitted error. In this assessment, a threshold of $\pm 1\%$ has been utilized as an example, to compare the number of stations needed to achieve this precision of the result with respect to the actual value.

$$Error = \frac{P_n - P_{150}}{P_{150}} 100 \tag{3.4}$$

Figures 3.3(a) 3.3(b) display a negative error in the calculations for low values of number of stations, meaning for these values, the propeller provides higher thrust demanding more torque. In case of 3.3(c), it is displayed that the error is positive and therefore, the tool provides higher efficiencies than the real value. There is a common trend in the three pictures, that a cosine distribution converges more rapidly with less number of stations than the uniform distribution. In fact, a threshold of $\pm 1\%$ error is achieved for less than 10 stations if they are distributed according to the law described in equation 3.2 for thrust and torque cases, and even less for the case of efficiency. A uniform distribution of stations is remarkably worse in this terms, as the error threshold is obtained using more than 30 stations for thrust and torque. In terms of efficiency, the threshold is obtained with less stations, however, the cosine distribution is definitely better.

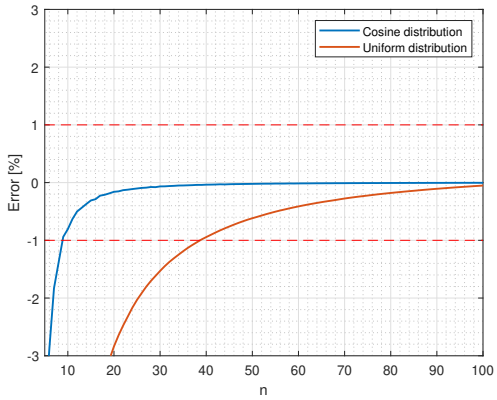

(a) *Thrust error vs J.*

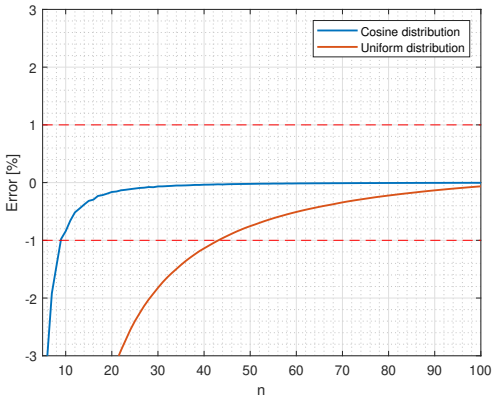

(b) *Torque error vs J.*

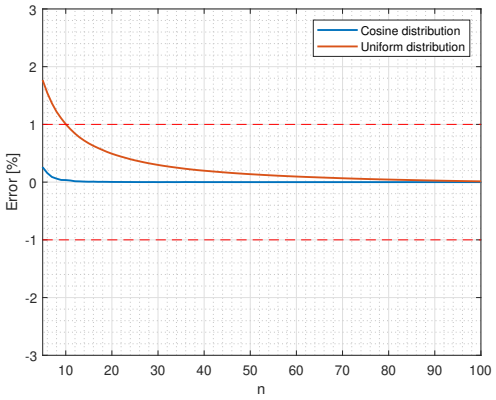

(c) *Efficiency error vs J.*

Figure 3.3: Number of stations effect

3.2 Cut-off ratio study

Cut-off ratio is the blade percentage at which the first station is placed. The whole propeller disk is not providing thrust as there is the hub in its centre which does not contribute to the performance. The presence of this hub is taken into account with the cut-off ratio. In this section, an assessment of the effect of the placement of the first station, that corresponding to a spatial $\xi_{\text{cut-off}}$ position, is performed. For this study, the same propeller of the previous Section 3.1 was used. In this case, the cosine law of distribution of stations was used with 60 stations (so that, for low values oh $\xi_{\text{cut-off}}$, the density of stations at the root was enough according to figures of Section 3.1, since low density of stations close to the root could mask the results for low values of $\xi_{\text{cut-off}}$) and the cut-off ratio was introduces as a parameter.

Figures 3.4, 3.5 and 3.6 display the curves of thrust, torque and efficiency versus advance ratio for different values of $\xi_{\text{cut-off}}$. It can be seen that, for values up to 30% thrust and torque are very similar and little error is incurred in, while for efficiency, the difference cannot be perceived.

Figures 3.4(b), 3.5(b) and 3.6(b) contain the curves for thrust, torque and efficiency for values from 35% up to 55%. In this case, a non negligible difference is found at J = 0.5 for thrust and at J = 0.6 for torque, these differences become smaller as J increases or diminishes.

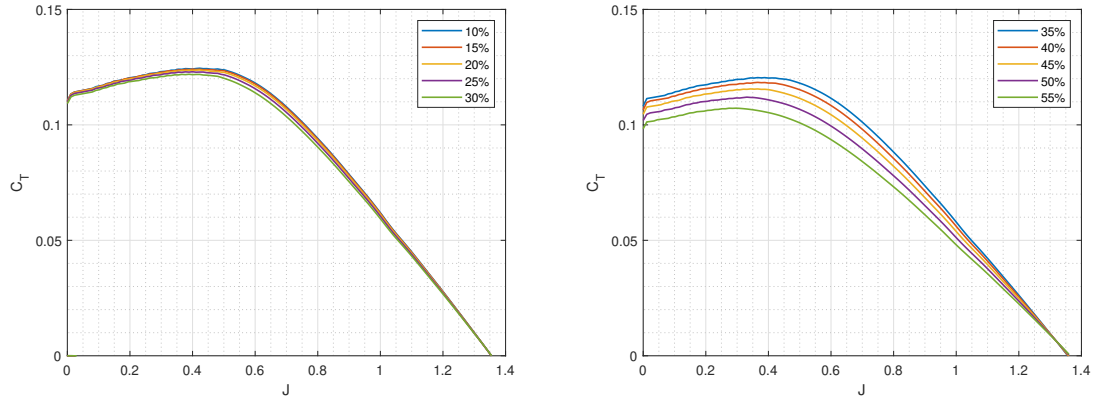

(a) (b)

Figure 3.4: Influence of cut-off ratio in C_T

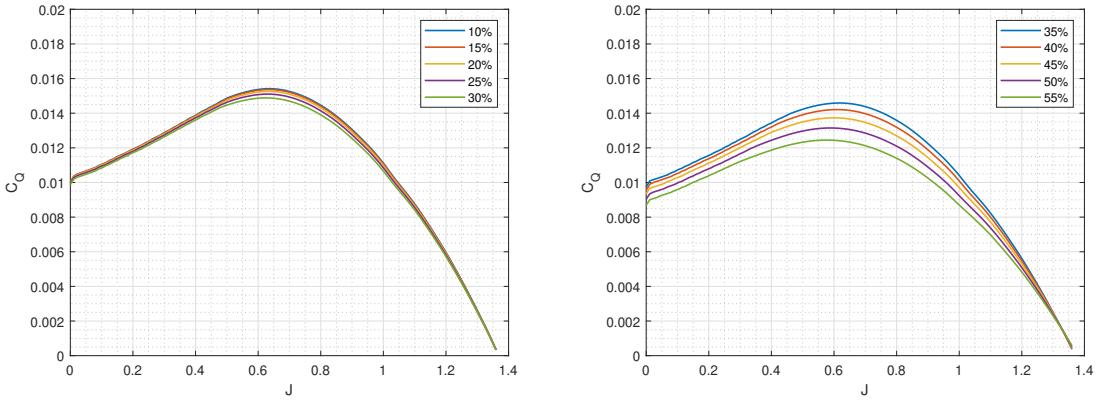

(a) (b)

Figure 3.5: Influence of cut-off ratio in C_Q

On the other hand, as it was anticipated, efficiency is virtually not altered.

Since the maximum of the difference in the final value for thrust and torque occurs at around half of the working interval of J of the propeller, an analysis of the loading of the blade was performed in order to assess the maximum error incurred by using one value of $\xi_{\text{cut-off}}$ or another. 3.7(a) shows the horizontal force coefficient distribution (see equation 2.33) along the span, while 3.7(b) the value of thrust at the station, proportional to the product of C_X by W^2 and the value of chord at the station (equation 2.1). In this figure, it can be seen both tip losses and that stations near the blade tip provide higher values of thrust. Finally, Figure 3.7(c) displays for each station the sum of the thrust of the sections up to that station, providing cumulative curves that reach the total value of thrust obtained at $\xi = 1$.

In Figure 3.7, curves for different values of $\xi_{\text{cut-off}}$ are provided. In the case of Figure 3.7(c), a dashed red line represent, as in Figure 3.3, the difference of 1%. $\xi_{\text{cut-off}}$ values of less than 20% provide values within the range of -1% (in the range of maximum difference; for other values of J, the difference is minor and higher values of $\xi_{\text{cut-off}}$ should be admitted).

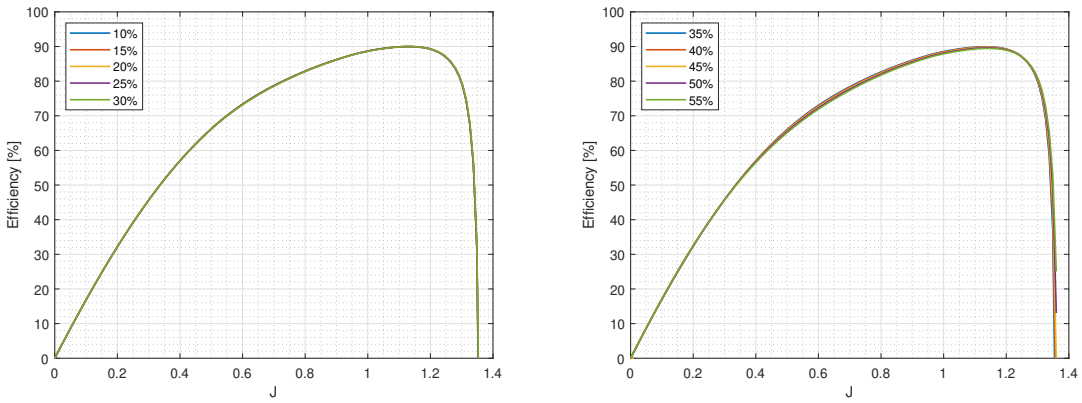

(a) (b)

Figure 3.6: Influence of cut-off ratio in η

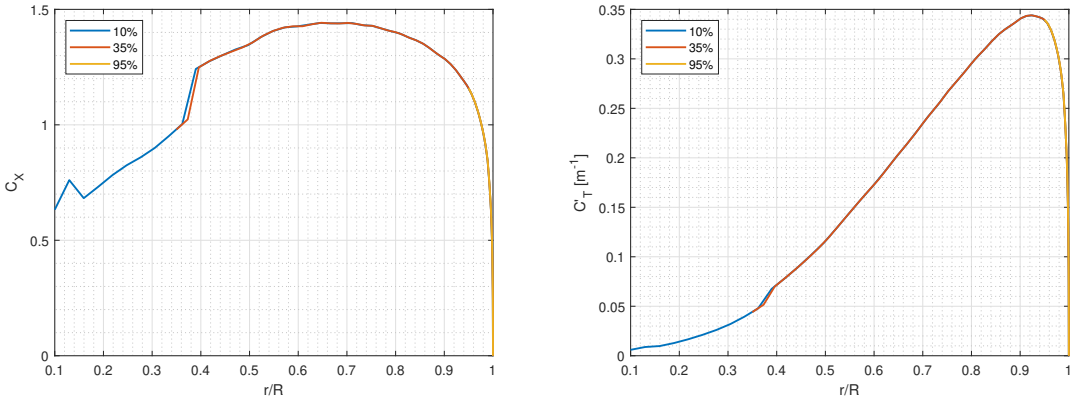

(a) C_X *vs* ξ (b) dT *vs* ξ

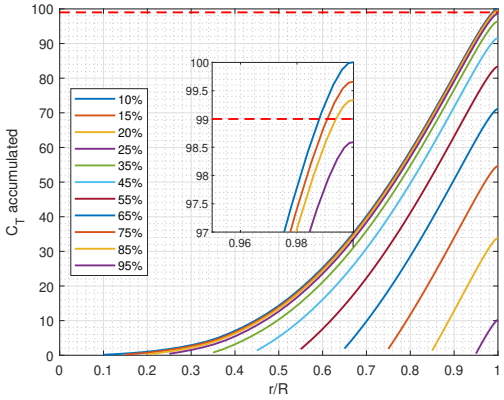

(c) dT *accumulated vs* ξ

Figure 3.7: Blade loading at J = 0.5

Chapter 4

Optimization studies

In this chapter the benefit of having a tool that calculates propeller performance in any condition is exploited. As it was mentioned, it is possible that fixing flight conditions, the parameters that define propeller geometry are changed until an arbitrary cost function is minimized.

Two different kinds of propeller optimizations will be performed for an 19-passenger commuter for which cruise and take-off phases are here detailed:

- Cruise design point:
  - Altitude 8000 ft.
  - True airspeed 115 m/s.
  - Power required 1500 kW
- Thrust requirements at take-off:
  - 54 kN at 31m/s.

The optimization routines here described focus mainly in obtaining high efficiency at cruise conditions. However, any kind of optimization problem could be formulated, like minimizing the size of the propeller or even, after the definition of such parameters, the minimization of working associated noise of the propeller.

As an initial guess for propeller sizing, the propellers mounted in aircraft Beech 1900 and Do-228 were considered as they are similar airplanes to the one described before. These two commuters obtain thrust with two engines that mount a propeller each, therefore, the restrictions of power required and thrust at take off are divided by two in the calculations performed.

4.1 Optimization variables and algorithm description

The parameters that permit obtaining propeller performance modifications were described in the previous chapters. Propeller geometry is defined after the diameter (D), airfoil of the section (such as RAF6 or NACA 4412 of Section 2.2 and Section 2.3 respectively), number of blades (B), twist and chord distributions (β and c).

In these optimization studies, airfoil of the section is not considered to be an optimization variable since a database of the aerodynamic coefficients must be computed and ready before

any calculation is performed. Also, the routine for the optimization utilized does not allow integer optimization, therefore, several optimizations in which number of blades was set constant at the beginning of each optimization were performed.

Continuing with parameters that define propeller geometry, in his thesis, Tarraran developed the optimum propeller for a drone, utilizing second grade polynomial expressions that defined twist and chord distributions [3]. These polynomials were defined by only three parameters, and thus, require little effort to implement in the code. Another advantage of using polynomial expressions is that only three variables are considered to be variables of optimization. However, other methods that define curves can be utilized. In fact, in this thesis, Bézier curves are exploited, as they are simple to introduce, and have been used in many engineering fields, including optimization of wind turbines [11]. Bézier curves are defined by a set of control points, $\mathbf{P_0}$ to $\mathbf{P_N}$, where N is the order of the curve. These control points here described are the variables of optimization that were considered.

$$\mathbf{B}(t) = \sum_{i=0}^{N} \mathbf{P}_i \mathbf{b}_{i,N}(t), \quad t \in [0,1] \tag{4.1}$$

where

$$\mathbf{b}_{i,N}(t) = \binom{N}{i} t^i (1-t)^{N-i}, \quad i = 0, 1, ..., N \tag{4.2}$$

These curves start and finish in control points $\mathbf{P_0}$ and $\mathbf{P_N}$. Figure 4.1 displays three Bézier curves that start and finish in the same control points but are of different orders. As it can be seen, higher order curves provide more complex shapes. In this thesis, three order curves defined by four control points were utilized, since no more complexity is needed.

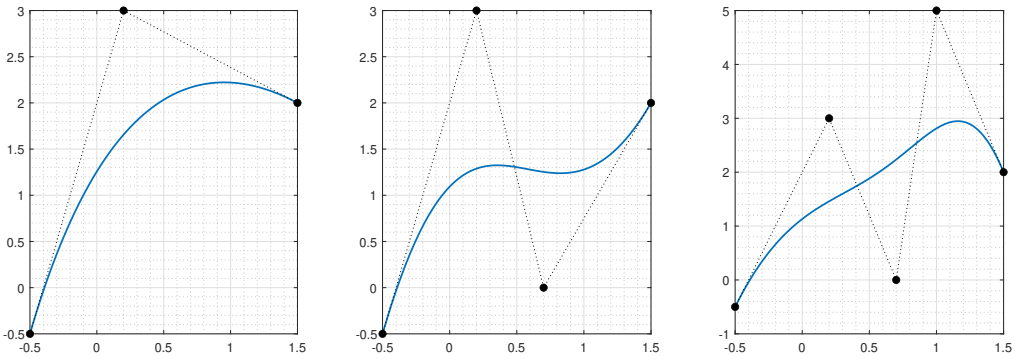

Figure 4.1: Different Bézier curves and control points

In summary, the total eighteen optimization variables of the problem are:

Optimization variables:
- 4x abscissa chord control points
- 4x ordinate chord control points
- 4x abscissa twist control points
- 4x ordinate twist control points
- D
- RPM

In the optimization performed in Section 4.4.1, two initial guesses for optimal geometry were considered: The first one, present in Table 4.1 provides linear chord and linear twist distributions and the second one, that of Table 4.2, constant chord and linear distribution of twist angle. For twist and chord distributions, the initial values of Bézier control points were considered such that two different twist and chord distributions could be defined:

Table 4.1: First initial geometry

	Chord		Twist	
	X	Y	X	Y
B0	0.200	1.250	0.200	60
B1	0.466	0.833	0.466	46
B2	0.733	0.416	0.733	32
B3	1.000	0.000	1.000	20

Table 4.2: Second initial geometry

	Chord		Twist	
	X	Y	X	Y
B0	0.200	0.750	0.200	60
B1	0.466	0.750	0.466	46
B2	0.733	0.750	0.733	32
B3	1.000	0.750	1.000	20

And 2.5 meters of diameter along with 2000 RPM.

In the problem described in equation 4.3, the minimum of a function is found taking into consideration six different kinds of constraints. The first array of constraints are the linear inequality constraints, defined by a matrix (A) and a vector (b). The second group is related to the linear equality constraints, again defined by a matrix (Aeq) and a vector (beq). The third and fourth groups of constraints are the non linear inequality and equality constraints respectively, that are imposed by the user. Finally, fifth and sixth groups of constraints are directly related to the domain of the parameters utilized, as they define the boundaries of the parameters. The routine that provides propeller optimization based on the minimization problem is described deeply in [**?**]:

$$\min_x f(x) \text{ such that } \begin{cases} A \cdot x & \leq & b \\ Aeq \cdot x & = & beq \\ nonlc & \leq & 0 \\ nonlc & = & 0 \\ lb & \leq x \leq & ub \end{cases} \tag{4.3}$$

In order to completely define the optimization problem, it is necessary to define a cost function (f(x), described in Section 4.2), the variables of optimization and the constraints (4.3).

There are also several options when choosing the optimization routine. There exists different kind of algorithms, such as the one called but after an exploration on the quality of the results provided by those different algorithms, a gradient-descent sequential quadratic programming (SQP) algorithm was chosen. This algorithm is also utilized by Sartori in [11] in an optimization problem similar to the one that is discussed in this thesis. For this algorithm, several parameters can be changed, for example the minimum size of change in the variables optimization between iterations. The influence of this parameter in the results has been analysed in Appendix B.

4.2 Cost functions

Here, the possibility of choosing any kind of cost function is exploited and two different optimizations were performed and discussed in Subsection 4.2.1 and Subsection 4.2.2.

4.2.1 Cruise performance optimization

In this case, cruise efficiency optimization is performed by calculating the efficiency at 115m/s of true incoming airflow speed. The variables of optimization are the eight parameters of the control points for chord distribution, symmetrically, eight points for twist distribution, diameter and rotational speed of the propeller. In this case, the function that provides the value of the cost function is quite simple:

1. Bézier control points are transformed into curves
2. Performance is calculated in cruise conditions
3. Cost function value is computed through equation 4.4

As it was mentioned, the optimization routine searches the minimum of a function, therefore, in order to obtain the maximum of the efficiency, the value of η_{cruise} must be changed of sign.

$$CF = -\eta \tag{4.4}$$

4.2.2 Wider interval of high efficiency

In this case, a loss in optimal cruise efficiency is admitted in exchange of a wider range in terms of advance ration in which the efficiency is higher than a desired tolerance. This is given by parameter γ, and the weight that high efficiency range of J has in the cost function is controlled by parameter κ. In this case, cost function value is obtained through 4.5. The cost follows these steps:

1. Bézier control points are transformed into curves
2. Performance computed multiple times in a range of speeds
3. η_{maximum} is found
4. J_{min} and J_{max} are obtained

5. ΔJ is computed

6. Cost function value is computed through equation 4.5

Setting $\gamma = 0.95$ will provide a interval of J in which the efficiency is higher than 95% of η_{max}, complying with the restrictions of thrust at take-off and cruise.

$$CF = -(\eta + \kappa \Delta J) \tag{4.5}$$

This kind of multi-objective optimization for which a Pareto-like diagram, similar to that of Figure 4.2, can be performed, is the objective of this cost function. In this figure, each star would correspond to an optimization in which a different value of κ was used, obtaining lower maximum efficiencies for increasing values of κ.

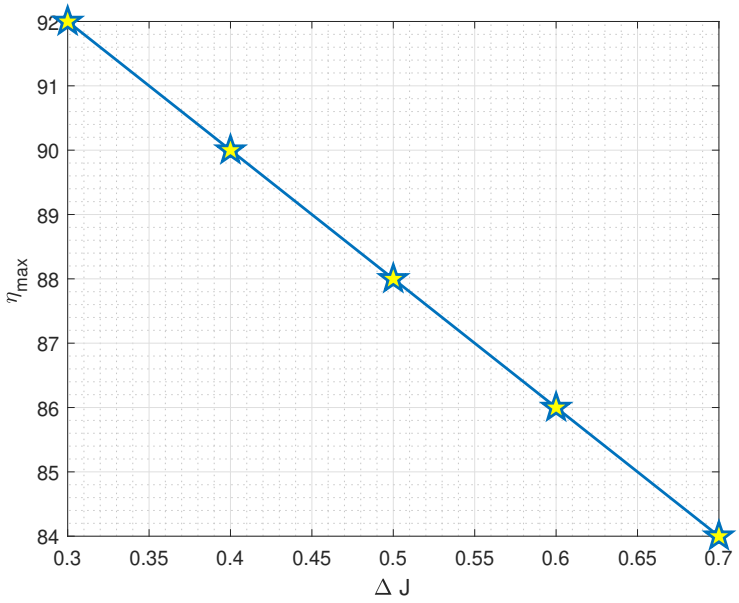

Figure 4.2: Example of Pareto diagram

4.3 Constraints

As described in equation 4.3, the minimization problem allows the inclusion of non linear constraints. Thanks to this, it is easy to implement required thrust values during different phases of the mission. In both optimizations performed, the next list summarizes the constraints imposed, following the nomenclature required by 4.3:

1. T_{TO} - $T_1 \leq 0$
2. T_{Cruise} -$T_2 \leq 0$
3. M_{tip} - $M_{lim} \leq 0$
4. Re_{min} - $Re_i \leq 0$
5. B_{x0_c} - $\xi_{cut\text{-}off} \leq 0$

6. B_{x0_t} - $\xi_{\text{cut-off}} \leq 0$

7. 1 - $B_{x3_c} \leq 0$

8. 1 - $B_{x3_t} \leq 0$

Restrictions number 1. and 2. represent thrust constraints during different phases of flight, as thrust at those phases must be higher to values prescribed at the beginning of the optimization. Constraint number 3. limits the maximum value of the Mach number at the blade tip to that of the maximum Mach number available in the database of polars. This constraint is directly limiting the diameter of the propeller, as higher speeds are encountered in the tip due to rotational speed. The other way around happens with constraint number 4; this constraint is actually a group of n constraints, being n the number of stations. They force that Reynolds number at each station is higher than the minimum Reynolds number present in the database. This constraint is particularly important as the curve that defines chord distribution may take lower than zero values between iterations of the optimization routine, leading to negative chords. Since Reynolds number is a function of the chord, negative chords would result in negative Reynolds number at the section and, following the procedure of Section 2.1.3, the routine would utilize the polars of the lowest Reynolds number available to obtain results, and therefore, the results obtained would not realistic as they come from unfeasible chords. Constraints 5. to 8. are related to the abscissa coordinate of the Bézier control points for both twist and chord distributions. They require that the first control point must be to the left of the first station and that the last control point must be to the right of the blade end, in order to have a single value of twist or chord at each station.

In summary, constraints 1 to 4 are contained in the non linear constraints group, while constraints 5 to 8 belong to the boundaries of the values that the optimization parameters can take.

4.4 Results

4.4.1 Cruise performance optimization

Two initial geometries to be optimized were considered. In the first case, linear chord and twist distributions along blade span, while in the second, constant chord and linear twist distributions are considered. Optimized propeller performance are confronted to those of the initial guesses in figures 4.5 and 4.7. Both optimizations are confronted in Figure 4.9. In all these figures, cruise and take off conditions are marked with dots of the colour of the line that correspond to the geometry from which it was obtained. Initial guesses of geometries are depicted along with their optimizations in figures 4.4 and 4.6 and the optimal geometries are confronted in 4.8. Figure 4.3 displays a breakdown of execution times. It reveals that most part of an optimization time is devoted to finding aerodynamic coefficients. This amount of time highlights the need of a faster method of providing aerodynamic data to the tool.

In terms of performance, Figure 4.5(c) shows a ten percent increment in efficiency at cruise, the quantity that was being optimized. In figures 4.5(a) and 4.5(b) a slight increment of thrust and torque coefficients curves with respect to J is present.

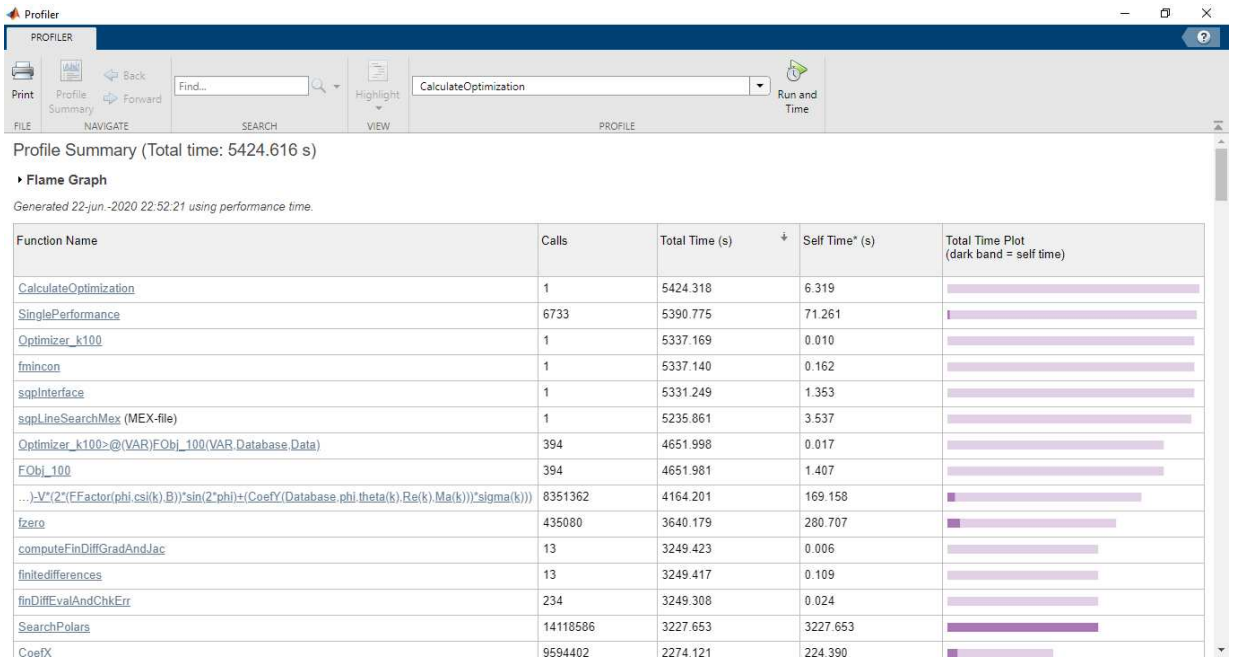

Function Name	Calls	Total Time (s)	Self Time* (s)	Total Time Plot (dark band = self time)
CalculateOptimization	1	5424.318	6.319	
SinglePerformance	6733	5390.775	71.261	
Optimizer_k100	1	5337.169	0.010	
fmincon	1	5337.140	0.162	
sqpInterface	1	5331.249	1.353	
sqpLineSearchMex (MEX-file)	1	5235.861	3.537	
Optimizer_k100>@(VAR)FObj_100(VAR,Database,Data)	394	4651.998	0.017	
FObj_100	394	4651.981	1.407	
...)-V*(2*(FFactor(phi,csi(k),B))*sin(2*phi)+(CoefY(Database,phi,theta(k),Re(k),Ma(k)))*sigma(k)))	8351362	4164.201	169.158	
fzero	435080	3640.179	280.707	
computeFinDiffGradAndJac	13	3249.423	0.006	
finitedifferences	13	3249.417	0.109	
finDiffEvalAndChkErr	234	3249.308	0.024	
SearchPolars	14118586	3227.653	3227.653	
CoefX	9594402	2274.121	224.390	

Figure 4.3: Optimization breakdown times

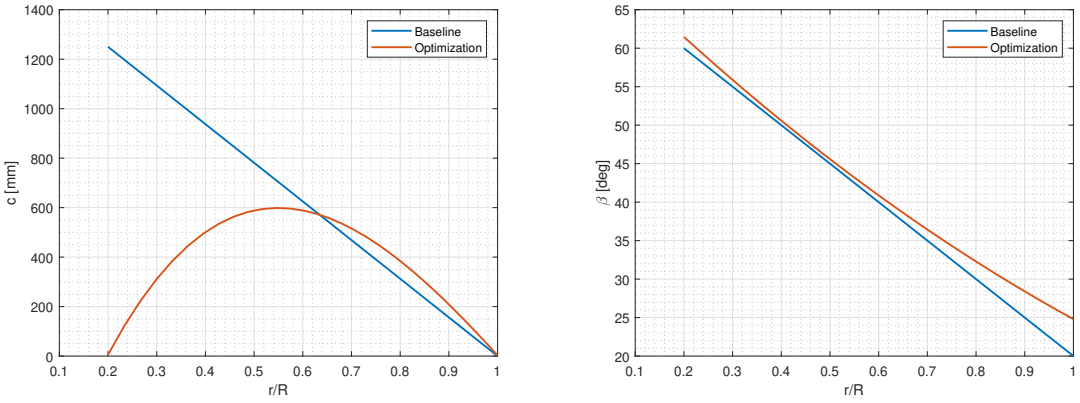

(a) *Chord distribution* (b) *Twist distribution*

Figure 4.4: Cruise-optimized propeller geometry - Case 1

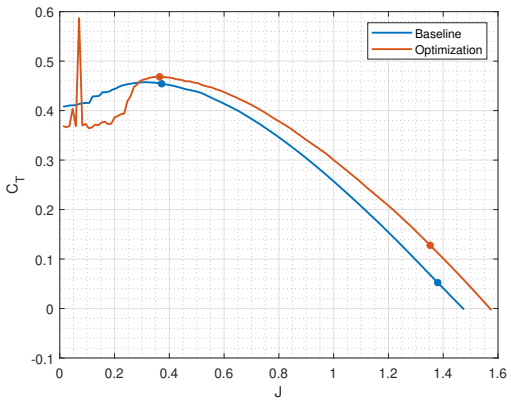

(a) C_T *vs* J.

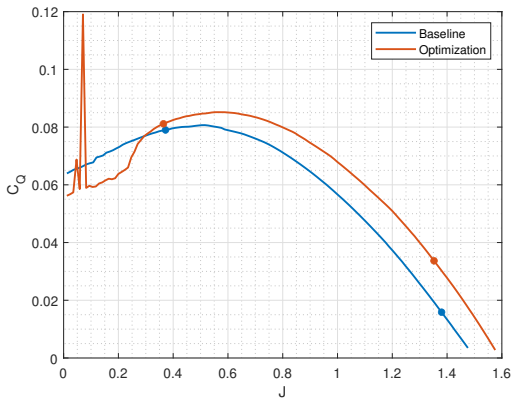

(b) C_Q *vs* J.

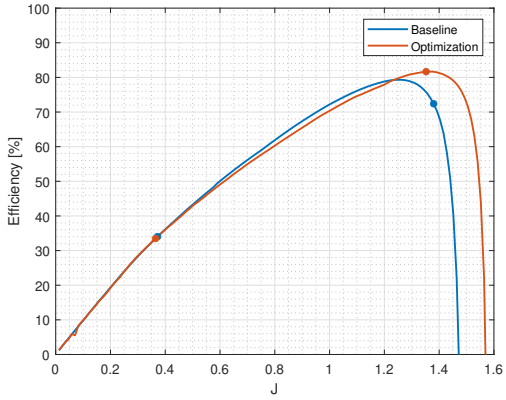

(c) η *vs* J.

Figure 4.5: Cruise-optimized propeller performance - Case 1

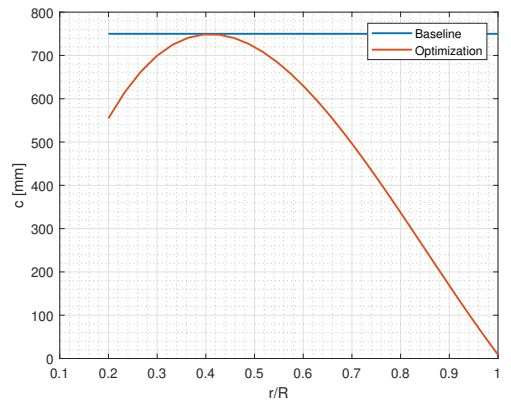

(a) *Chord distribution*

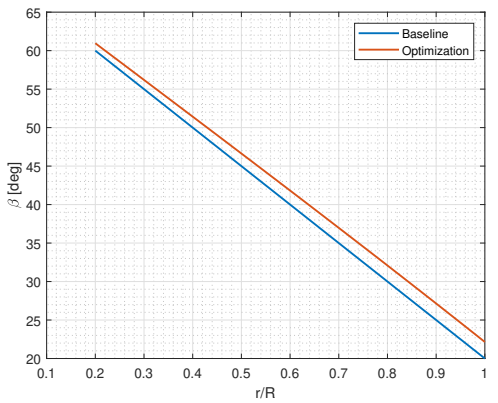

(b) *Twist distribution*

Figure 4.6: Cruise-optimized propeller geometry - Case 2

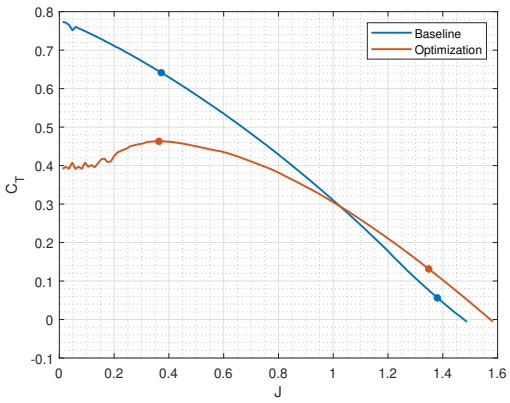

(a) C_T *vs* J.

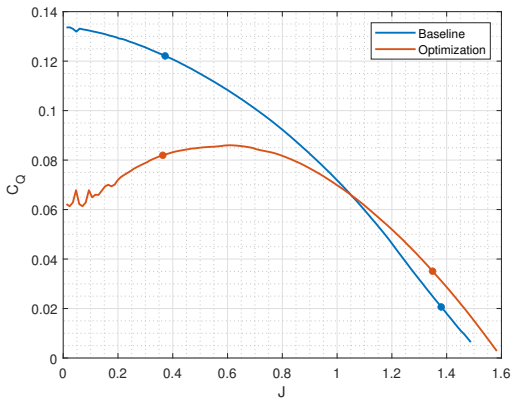

(b) C_Q *vs* J.

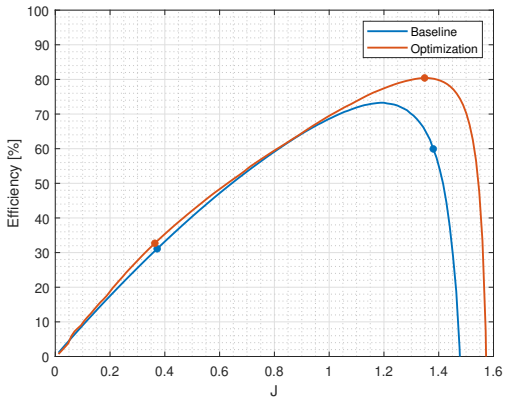

(c) η *vs* J.

Figure 4.7: Cruise-optimized propeller performance - Case 2

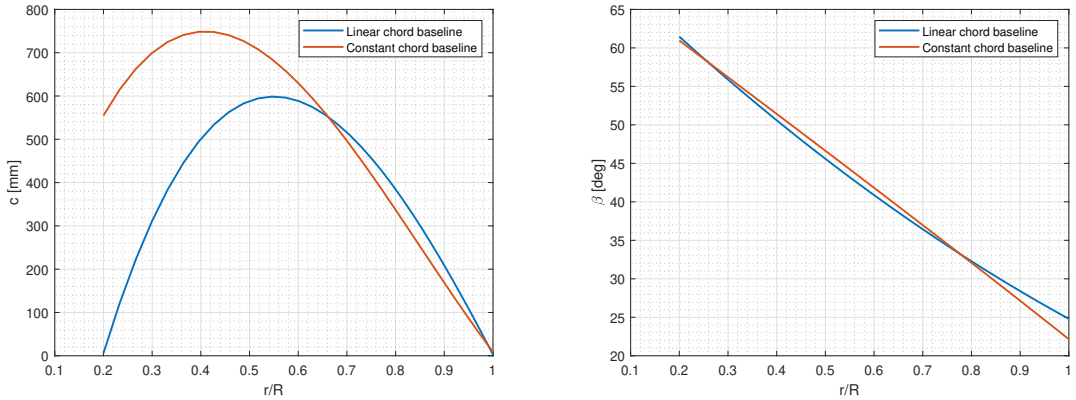

(a) *Chord distribution* (b) *Twist distribution*

Figure 4.8: Cruise-optimized propeller geometries comparison

It is remarkable that, in the initial guess of linear chord distribution in which at $\xi_{\text{cut-off}}$ a chord of 1.25 meters was present, the optimization led to a close to zero value of chord for that station, while, in the case of constant chord distribution, the value at that station is higher than 0.5 meters. Also, the point of maximum chord differs, being in one case before half of the blade and after in the other. However, in both cases, the chord is close to zero (and not precisely zero, as discussed in Section 4.3) at the tip. However, at a first glance, the optimal geometries coming from the optimization of a constant chord propeller are more feasible, since a not null chord is present at the hub limit.

Optimized twist distributions are quite similar with a slight change in the twist angle at the tip of the blade, meaning that, for this optimization, twist variables are of less importance in comparison with Bézier control points of chord distribution.

Quite different optimal geometries present in Figure 4.8 led to the performances present in 4.9. In fact, in these figures, very similar curves for thrust, torque needed and efficiency with respect to J were obtained. In Figure 4.9(a), two dashed red segments representing the constraints of thrust at take-off and cruise are present and, for the two constraints, both optimizations are compliant with the requirements.

In terms of efficiency, optimal values at convergence in the two optimizations performed increased the efficiency of their respective initial guesses, being their values almost equal. In any case, the efficiency at this maximum is slightly over 80%, a value that is not excellent. One cause of this "low" value for maximum efficiency at cruise could rely on the constraint of using NACA 0012 airfoil, the only airfoil for which aerodynamic coefficients at M = 0.84 were known. This symmetric airfoil needs higher angles of attack than other known airfoils to obtain the same lift coefficient and therefore, in order to satisfy the thrust constraints, large geometries that compromised efficiency were encountered. It is thought that a relaxation of these constraints could lead to higher efficiencies and the use of other airfoils could lead to higher cruise efficiency.

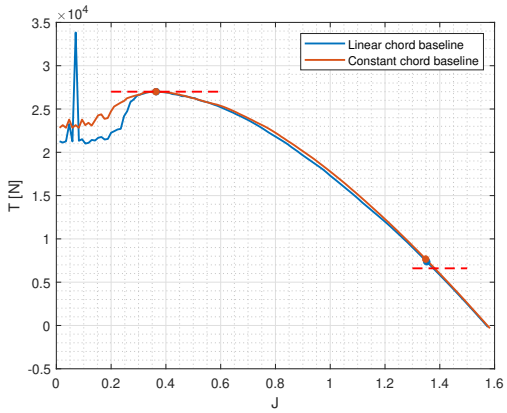

(a) C_T *vs* J.

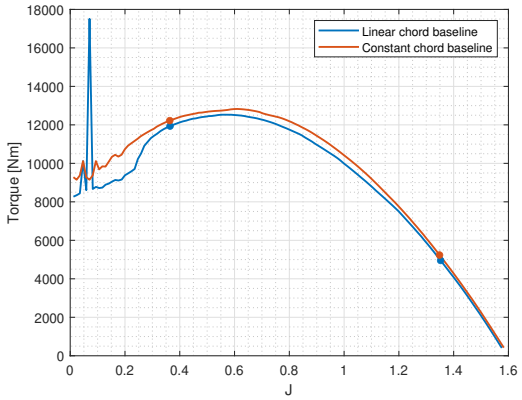

(b) C_Q *vs* J.

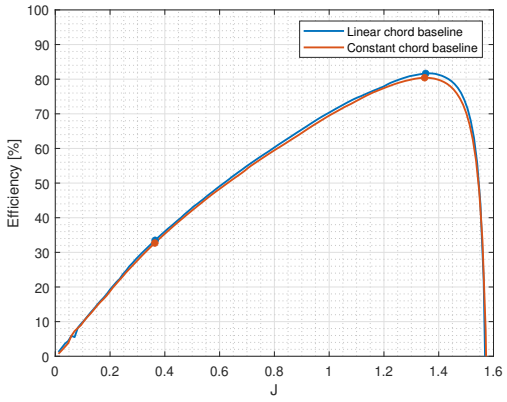

(c) η *vs* J.

Figure 4.9: Cruise-optimized propeller performances comparison

4.4.2 Wider interval of high efficiency

Unlike in Section 4.4.1 where two initial guesses of geometry were considered, in this section, only the propeller with linear chord and twist distributions was optimized, subjected to the cost function of described in Section 4.2.2. Referring to the parameters previously defined in that section, it was chosen a value for γ of 0.95, meaning that the interval of J introduced in the cost function takes into account those advance ratio values whose efficiency is higher than 95% of η_{max}. In this section, an assessment on the value of κ that permits the desired multi-objective optimization was performed.

Table 4.3 displays the results of different optimizations performed changing κ. This table presents the maximum of the efficiency curve, the range of advance ratio for which efficiency is higher than 95% and the percentage of total cost function devoted to increasing ΔJ. Initially, it was preferred that the contribution of the extended high-efficiency advanced ratio range was around 1% and 10% so that the optimization routine does not deviate from the initial target, η_{max}, while complying with constraints. For each row in Table 4.3, optimized geometries were obtained. Looking at Figure 4.12, for $\kappa = 0.35$, chord distribution adopted a non feasible shape. In fact, the rest of optimizations performed for κ values higher than 0.35 display similar trends of non feasible chord distributions at convergence.

Figure 4.10 displays the two contents of the cost function at convergence, not taking into

Table 4.3: Multi-objective optimization results

κ	η_{max} [%]	ΔJ	$\frac{\kappa \Delta J}{CF}$ [%]
0.000	81.69	0.2780	-
0.025	79.61	0.2868	0.89
0.050	81.07	0.2958	1.79
0.075	81.02	0.2947	2.65
0.100	81.02	0.2939	3.50
0.125	81.83	0.2909	4.25
0.150	81.54	0.2886	5.04
0.175	81.75	0.2720	5.50
0.200	81.07	0.3005	6.91
0.225	80.94	0.2962	7.60
0.250	80.95	0.2972	8.40
0.275	80.96	0.2977	9.18
0.300	81.55	0.3082	10.18
0.325	80.61	0.2996	10.77
0.500	78.25	0.2920	15.72
0.700	79.89	0.3110	21.41
1.000	78.09	0.3426	30.49

account the value of κ, but rather showing the desired ΔJ value in 4.10(a) and with the effect of the weighting parameter κ in 4.10(b). There are very small variations in the desired high efficiency interval, with a trend of increasing said interval for κ values higher than 0.35, the limit of feasible chord distributions. In fact, for low values of κ, the component $\kappa\Delta$J is relatively small, therefore, the proportion of $\kappa\Delta$J with respect to η_{max} should be higher in order to obtain a distinguishable improvement of this aspect. Optimal values of CF components for κ up to 0.35 makes it difficult to provide a Pareto curve similar to that of 4.2.

In any case, Figure 4.11 displays how total value of the cost function increases with the value of κ. The value of this cost function is not as relevant as in the case of cruise optimization but in this case, components that form the cost function and their proportion are more important, since their corresponding weight in the CF determine which will be more taken into account.

Figure 4.12 displays a sample of the kinds of geometries obtained in these optimizations. The yellow curve corresponds to the mentioned unfeasible distribution. Orange curve is, on the other hand, very similar to the optimization of cruise performance, due to the small κ value.

Looking at 4.13, relaxing the constraints for thrust at take off, those that are in the limit, could lead to an improvement of the chord distribution shapes, since large chord values would not be necessary, similarly as described in Section 4.4.1 for the previous optimization.

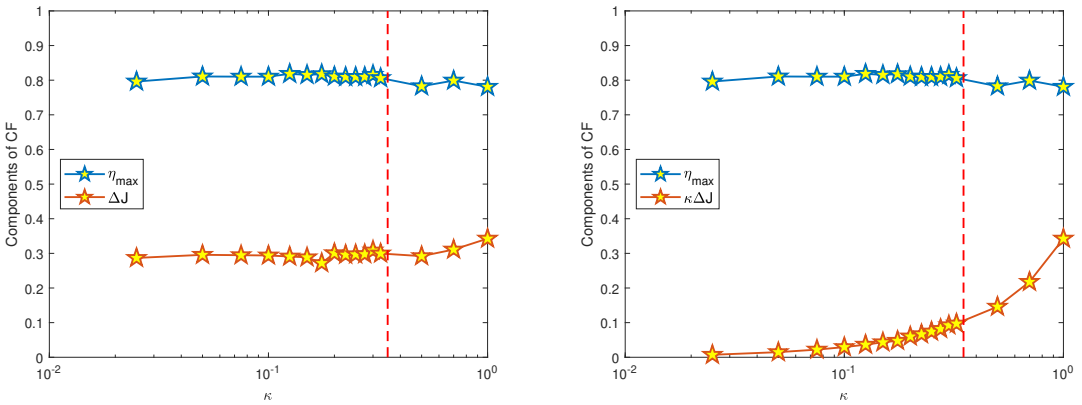

(a) *Without κ effect* (b) *With κ effect*

Figure 4.10: Cost function components at convergence

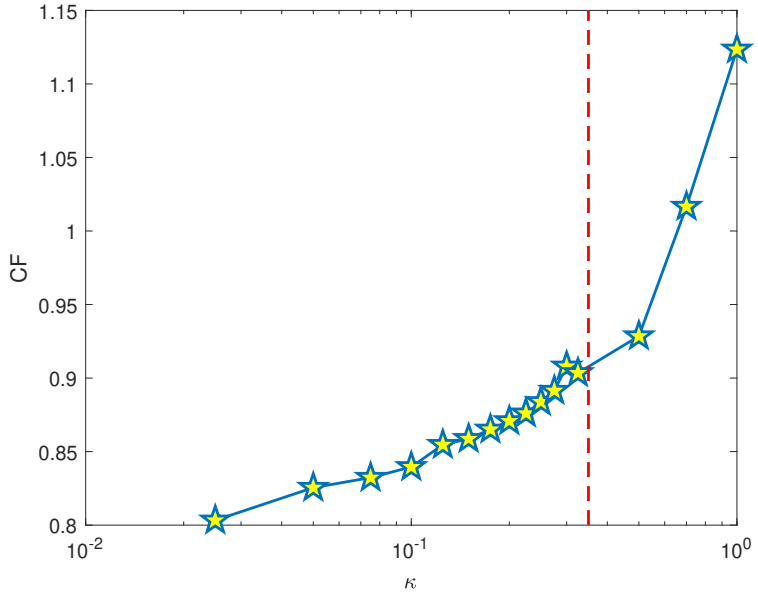

Figure 4.11: Cost function value at convergence

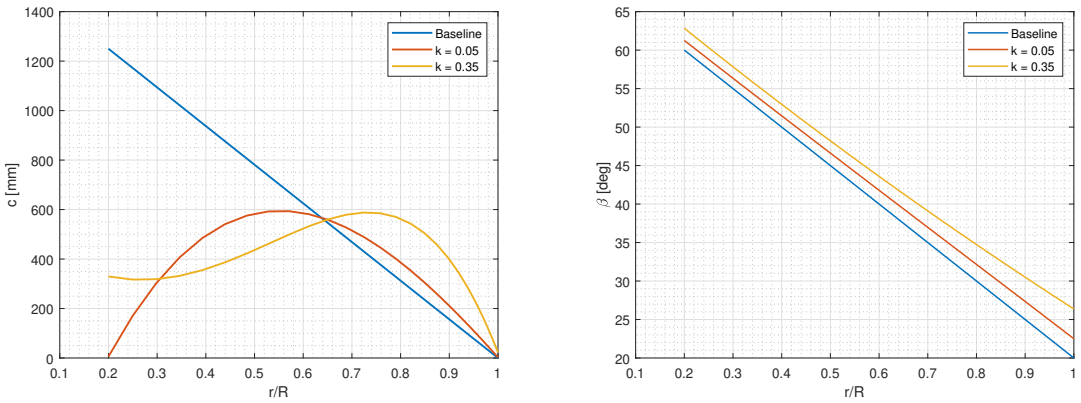

(a) *Chord distribution* (b) *Twist distribution*

Figure 4.12: Multi-objective-optimized propeller geometries

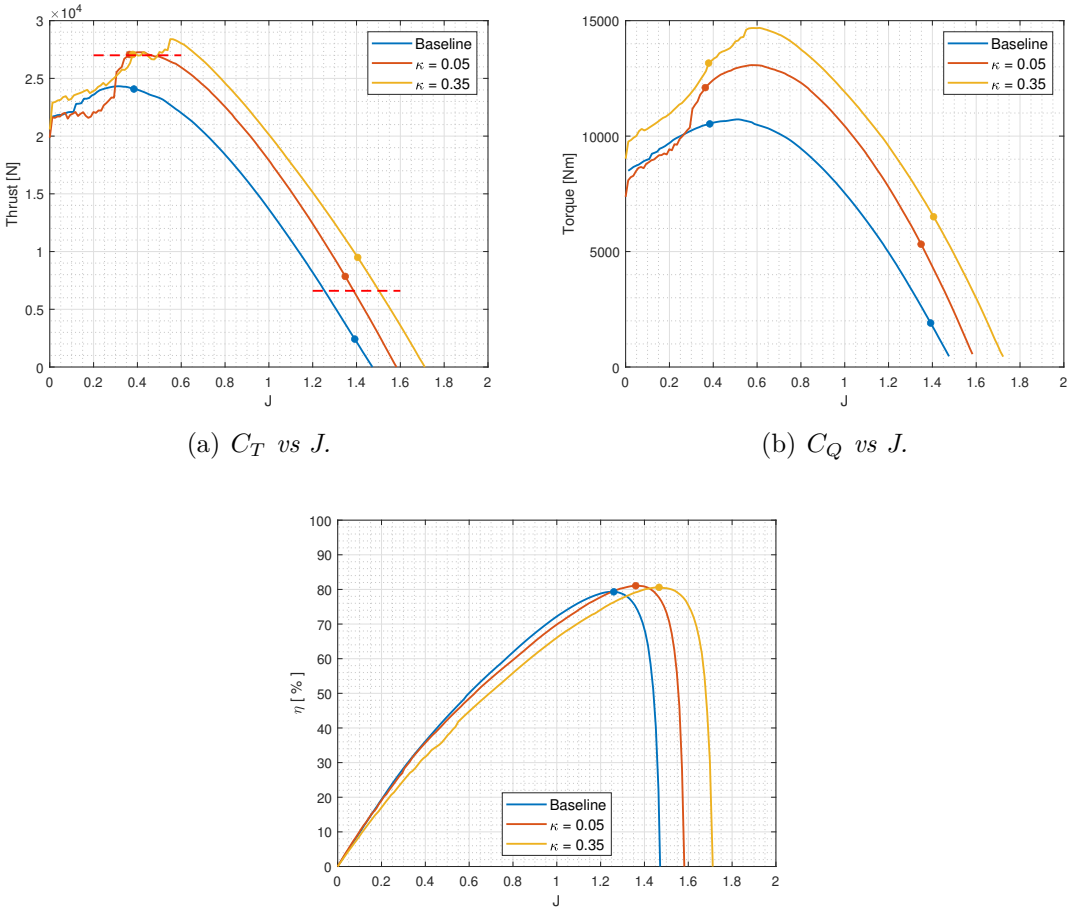

(a) C_T *vs J.* (b) C_Q *vs J.*

(c) η *vs J.*

Figure 4.13: Multi-objective-optimized propeller performances

Chapter 5

Conclusions and recommendations

5.1 Present work

The modelling of propeller performance has been a success: Firstly, in Chapter 2, the set of the BEMT equations that conform the model were presented. These equations are solved with the help of the method proposed by Ning in his article [12] and compared with other methods in Section 2.2. Later in this chapter, a validation of the calculations performed was carried by confronting the data provided by the tool with data obtained in tunnel testing of the propeller analysed in [1].

Once the model was properly constructed and reliable results were obtained, two numerical assessments were performed related to the influence of different parameters, that define propeller geometry, have in the quality of the solution. In Chapter 3, firstly, the study of number of stations revealed that depending on the kind of law for distribution of stations along the blade span, the number of stations needed to incur a small error changes. In fact, a cosine law distribution is better than a uniform law, since less stations are needed. Twenty stations and a cosine law distribution provide good results. Secondly, the first station location influence in the calculations was addressed. Figure 3.7(c) shows how up to a 20% of the blade span near to the root can be neglected in the calculations with very small error.

Finally, thanks to the modelling of propeller performance parametrically, achieved during the realization of this thesis, allowed to perform several optimization studies. In Chapter 4, in fact, two kinds of optimizations were performed. Firstly, two optimizations of propeller performance in cruise conditions for a 19-passenger commuter were performed for different values of initial geometry guesses. For these optimizations, a maximum efficiency of around 80% were encountered, evidencing the importance of the airfoil of the section an the constraints related to the minimization problem. Secondly, a multi-objective optimization study was performed with an assessment on the influence of parameter κ in the results. During this optimizations non feasible chord distributions were encountered, but the results are satisfactory.

5.2 Further studies

Regarding future studies for this work, other phenomena occurring during propeller operation can be introduced in the model. For example, this model lacks a description of the contraction of the slipstream in the wake. A model of noise and vibrations could be also introduced so that it can serve as a parameter in the optimization routines of quieter propellers.

Even though the modelling of propeller performance calculations was properly implemented and the quality of the results was good, there is still margin to improve.

1. In Section 2.1.3, the aerodynamics implementation is described. During Chapter 3, only data coming from XFOIL was needed, however, when performing optimizations in which high subsonic Mach numbers are reached, the addition of other data sources is required. It is thought that maximum efficiencies obtained in 4.4 could be higher using another airfoil, but to obtain this, the database of polars should be expanded for these new airfoils, as performed for the NACA 0012.

2. For low advance ratio values, thrust and torque curves display oscillations. At this conditions, a big amount of the blade is stalled and the aerodynamic coefficients are approximated with the Viterna method. This approximation could be enhanced by using other methods.

3. Continuing with the database extension, even though other databases of polars for different airfoils were here used, all the studies performed considered constant airfoil along the span. Including the capability of changing airfoil along the span could enhance optimization results.

4. Finding other ways of implementing the aerodynamics in the tool, by the use of approximations with correcting coefficients, could reduce the computational time, the main drawback of this implementation.

5. Appendix B contains the results of optimizations in which the option 'DiffMinChange' was changed. The influence of other parameters of the minimization routine in optimization results should be also studied, as very different propeller geometries lead to similar results in terms of performance.

Bibliography

[1] Xiang, S., "An improved propeller design method for the electric aircraft", *Aerosp. Sci. Technol.*, May 2018.
doi: https://doi.org/10.1016/j.ast.2018.05.008

[2] Glauert, H., "Airplane propellers" W. F. Durand, *Aerodynamic theory*, Farnborough, England, 1935.

[3] Tarraran, N., "Optimal approach to propeller design", M. Sc. thesis, Dipartimento di Scienze e Technologie Aerospaziali, Politecnico di Milano, 2018.

[4] Adkins, C. N., "Design of optimum propellers", Douglas Aircraft Company, *Journal of Propulsion and Power*, Vol. 10, No. 5, Sept.-Oct. 1994.
doi: https://doi.org/10.2514/3.23779

[5] Ning, A., "A simple solution method for the blade element momentum equations with guaranteed convergence", *Wind Energy*, Vol. 17, No. 9, pp. 1327-1345, Sep. 2014.
doi: https://doi.org/10.1002/we.1636

[6] Drela, M., "XFOIL - An analysis and design system for low Reynolds number airfoils", Mueller T.J. (eds) Low Reynolds Number Aerodynamics. Lecture Notes in Engineering, Vol. 54, Berlin, 1989.
doi: https://doi.org/10.1007/978-3-642-84010-4_1

[7] Viterna, L. A., and Corrigan, R.D., "Fixed pitch rotor performance of large horizontal axis wind turbines", NASA TR-19800310962, Cleveland, Ohio, Jan. 1982.

[8] Harris, C.D., "Two dimensional characteristics of the NACA 0012 airfoil in the Langley 8-foot transonic pressure tunnel". NASA TM-81927, Apr. 1981.

[9] Mahmuddin, F., "Airfoil lift and drag extrapolation with Viterna and Montgomerie methods", *Energy Procedia* 8th International Conference on Applied Energy, 2016.
doi: 10.1016/j.egypro.2017.03.394

[10] Angelo, S.D., Berardi, F. and Minisci, E., "Aerodynamic performances of propellers with parametric considerations on the optimal design", *Aeronautical Journal* Vol. 106 Issue 1060, pp. 313–320, Jun. 2002.
doi: https://doi.org/10.1017/S0001924000096068

[11] Sartori, L., "System design of lightweight wind turbine rotors", Ph.D. Dissertation, Dipartimento di Scienze e Technologie Aerospaziali, Politecnico di Milano, Jan. 2019.

[12] Hwang, J.T., and Ning, A., "Large-scale multidisciplinary optimization of an electric aircraft for on-demand mobility", AIAA Structures, Structural Dynamics, and Materials Conference, Kissimmee, FL, Jan. 2018.
doi: 10.2514/6.2018-1384

Appendix A

Pseudocode

This chapter contains a summary of the functions used to develop the tool. In order to be as much as understandable as possible, but also to reduce space, it has been chosen to show this pseudocode rather than MATLAB language directly.

Function: SinglePerformance

Input: Aerodynamics, Geometry, Conditions.
Result: η, T, Q, C_T, C_Q
Result: ϕ, C_X, C_Y, a, a', AoA, dT, dQ

σ
c
β

while $\epsilon \leq \epsilon_{max} \ \wedge \ iter \geq iter_{max}$ **do**
    for $i < n$ **do**
        Re
        M
        solve $f_{ref}(\phi) = 0$
        $C_{X_i} = f(\phi)$
        $C_{Y_i} = f(\phi)$
        $F_i = f(\phi)$
        $a_{ix} = f(\phi)$
        $a_{ix} = f(\phi)$
    end
    $\epsilon = \epsilon_{new}$
end

$dT = f(C_X)$
$dQ = f(C_Y)$

$T = \text{trapez}(dT)$
$Q = \text{trapez}(dQ)$
$\eta = \frac{TV}{\Omega Q}$

end SinglePerformance

Function: C_X

Input: Aerodynamics, Geometry, Conditions.
Result: C_X

Compute AoA

if *AoA* $\in$ *AoA database* **then**
  call SearchPolars
  call InterpolatePolars
else
  if *AoA* = AoA_{max} + *margin* $\|$ *AoA* = AoA_{min} - *margin* **then**
    call SearchPolars
    call ViternaMethod
    Weighted average: [Database ; Viterna]
  else
    call ViternaMethod
  end
end

$C_X = C_L \cos\phi$ - $C_D \sin\phi$

end C_X

Function: C_Y

Input: Aerodynamics, Geometry, Conditions.
Result: C_X

Compute AoA

if *AoA* $\in$ *AoA database* **then**
    call SearchPolars
    call InterpolatePolars
else
    if *AoA* = AoA_{max} + *margin* || *AoA* = AoA_{min} - *margin* **then**
        call SearchPolars
        call ViternaMethod
        Weighted average: [Database ; Viterna]
    else
        call ViternaMethod
    end
end

$C_Y = C_L \sin\phi + C_D \cos\phi$

end C_Y

Function: SearchPolars

Input: PolarDatabase, Re, M.
Result: UpperReUpperM, LowerReUpperM, UpperReLowerM, LowerReLowerM

Find the two closer Re numbers in database.
Compute difference to that numbers.

Find the two closer M numbers in database.
Compute difference to that numbers.

end SearchPolars

Function: InterpolatePolars

Input: UpperReUpperM, LowerReUpperM, UpperReLowerM, LowerReLowerM, distances, ϕ, θ
Result: C_L, C_D

Compute AoA
Find the two closer AoA numbers in database.
Compute difference to that numbers.
Compute weighted average of the eight couples of C_L and C_D

- Four weighted average computations for AoA
- Two weighted average computations for Re
- One weighted average computation for M

end SearchPolars

Function: BezierCurve

Input: Control points
Result: X and Y vector coordinates of Bezier curve defined by control points

t = 0:0.001:1
binomial
Bernstein
sum binomial Bernstein
X
Y

end Bezier2Cosine

Function: Bezier2Cosine

Input: Cut-off ratio, number of stations, Bezier control points of twist and chord distributions
Result: Twist and chord distributions vectors

call BezierCurve (control points for twist)
call BezierCurve (control points for chord)
call CosineDistribution (Cut-off ratio, number of stations)

Discard twist and chord curve points that do not belong to CosineDistribution

end Bezier2Cosine

Function: CosineDistribution

Input: Cut-off ratio, number of stations
Result: Vector of spatial distribution of stations along the blade

for *i = 1:number of stations* **do**
  Compute eq 3.2
end

end CosineDistribution

Function: CostFunction1

Input: Optimization variables, Aerodynamic database, Geometry
Result: η_{obj}

call: Bezier2Cosine
call: SinglePerformance

$\eta_{obj} = -\eta_{cruise}$
end CostFunction1

Function: CostFunction2

Input: Optimization variables, Aerodynamic database, Geometry
Result: J_{obj}

call: Bezier2Cosine

for $J = J_1{:}J_2$ **do**
  call: SinglePerformance
  η_{J_i}
end
ΔJ = J $\in$ [J_{max}(1-γ), J_{max}(1+γ)]
$J_{obj} = -(\eta_{max} + k\Delta J)$

end CostFunction2

Appendix B

DiffMinChange

This chapter contains a brief summary of the optimizations performed to η_{cruise} by changing the minimum value of the steps in optimization variables in the gradient based minimization routine, *DiffMinChange*, for different initial guesses of propeller geometry, constant and linear chord distributions respectively. Figures B.1, B.4 and B.7 reveals that for very small values of *DiffMinChange*, (10^{-7} and 10^{-8}), optimal results at convergence (optimal geometry and η_{cruise}) in both cases is to that of *DiffMinChange* equal to zero. During this thesis, the default value for *DiffMinChange* was then kept to zero.

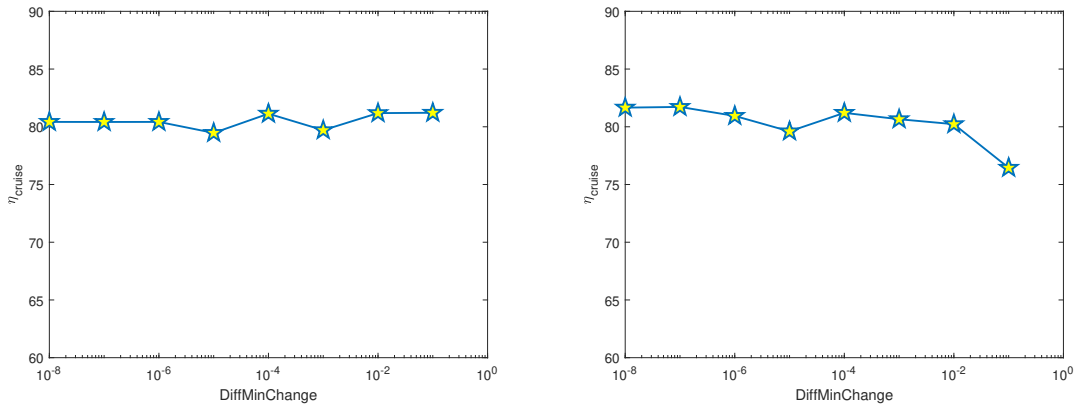

(a) *First initial guess* (b) *Second initial guess*

Figure B.1: η_{cruise} vs *DiffMinChange*.

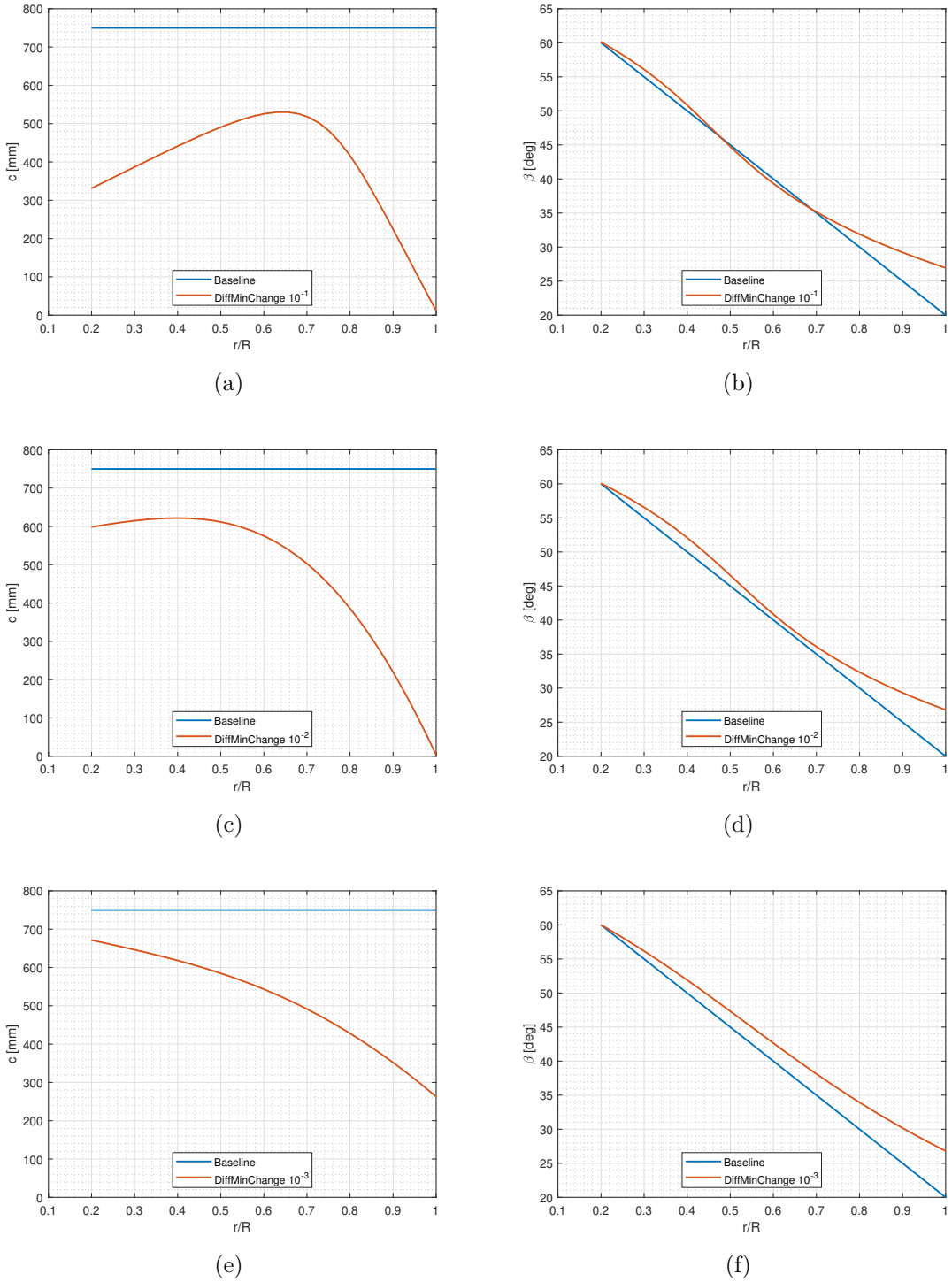

Figure B.2: Optimal geometries. First initial guess - 1 (3)

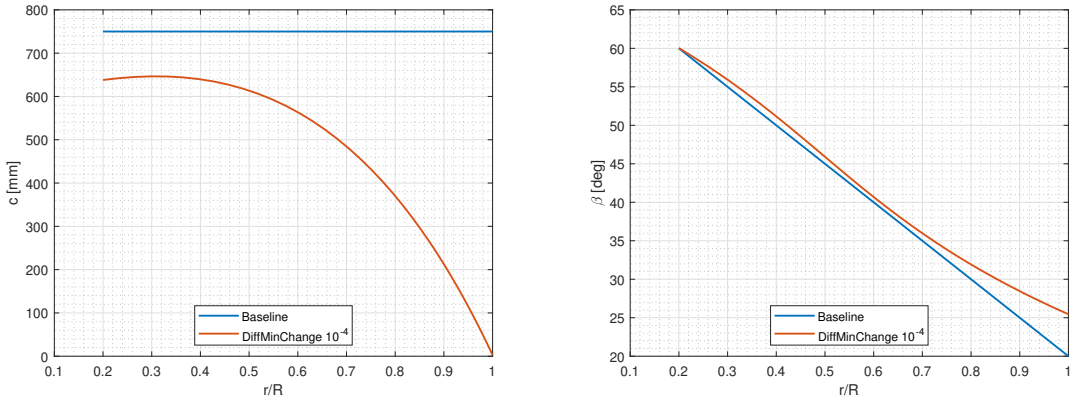

(a)

(b)

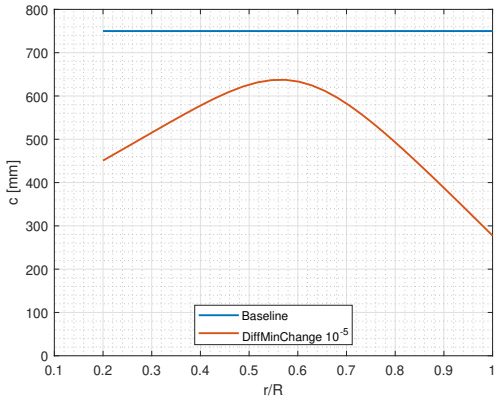

(c)

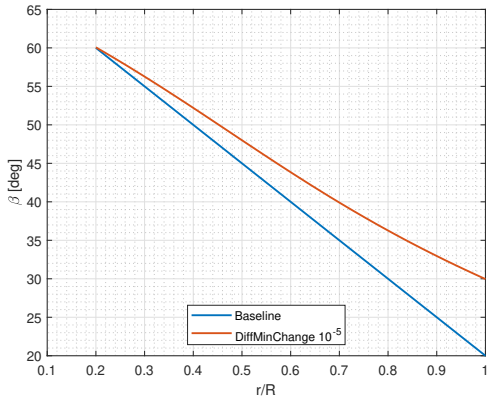

(d)

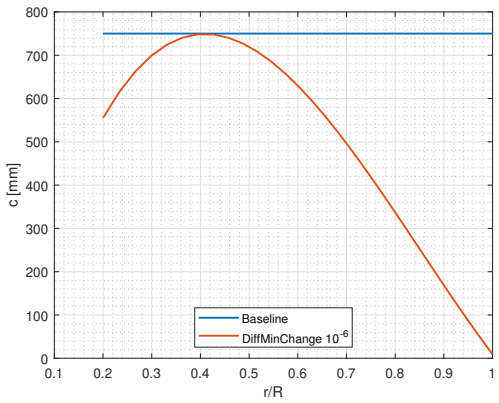

(e)

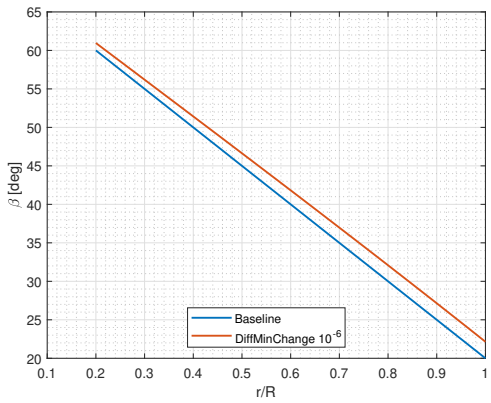

(f)

Figure B.3: Optimal geometries. First initial guess - 2 (3)

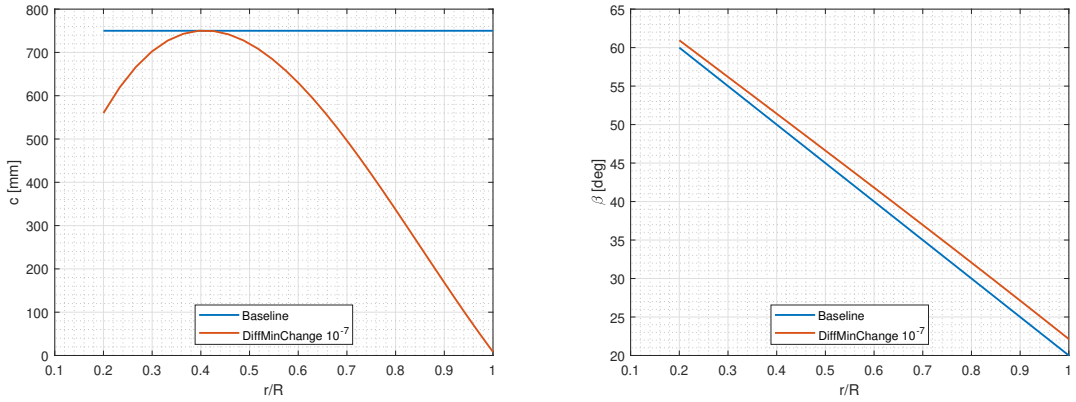

(a)

(b)

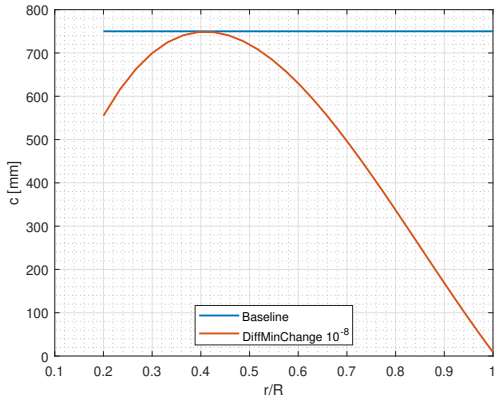

(c)

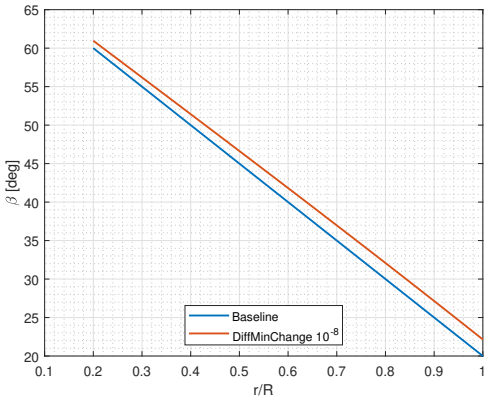

(d)

Figure B.4: Optimal geometries. First initial guess - 3 (3)

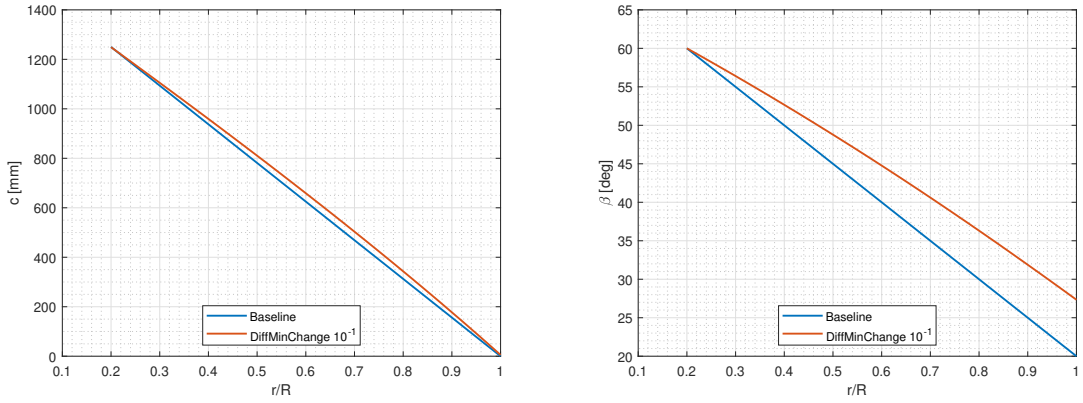

(a)

(b)

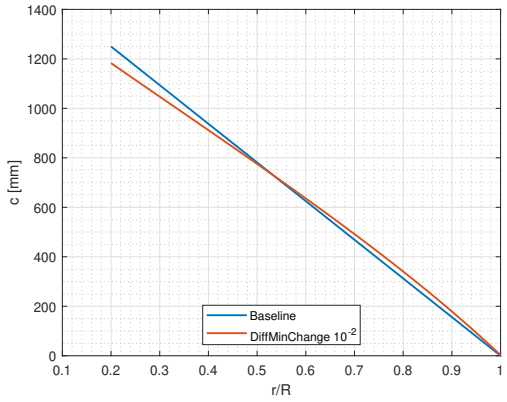

(c)

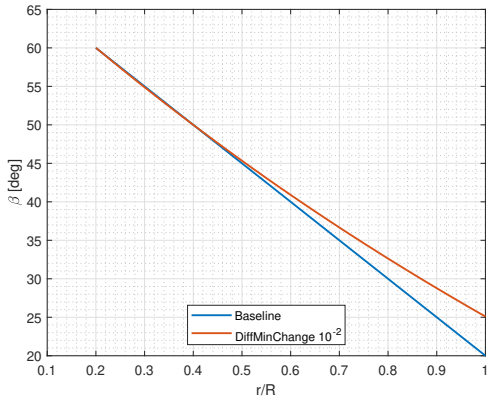

(d)

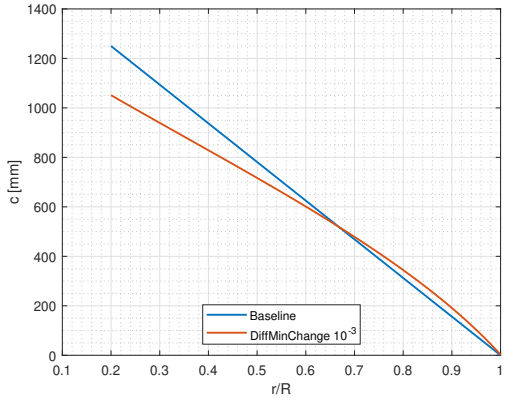

(e)

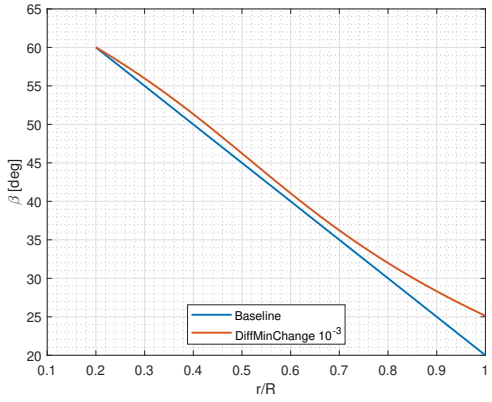

(f)

Figure B.5: Optimal geometries. Second initial guess - 1 (3)

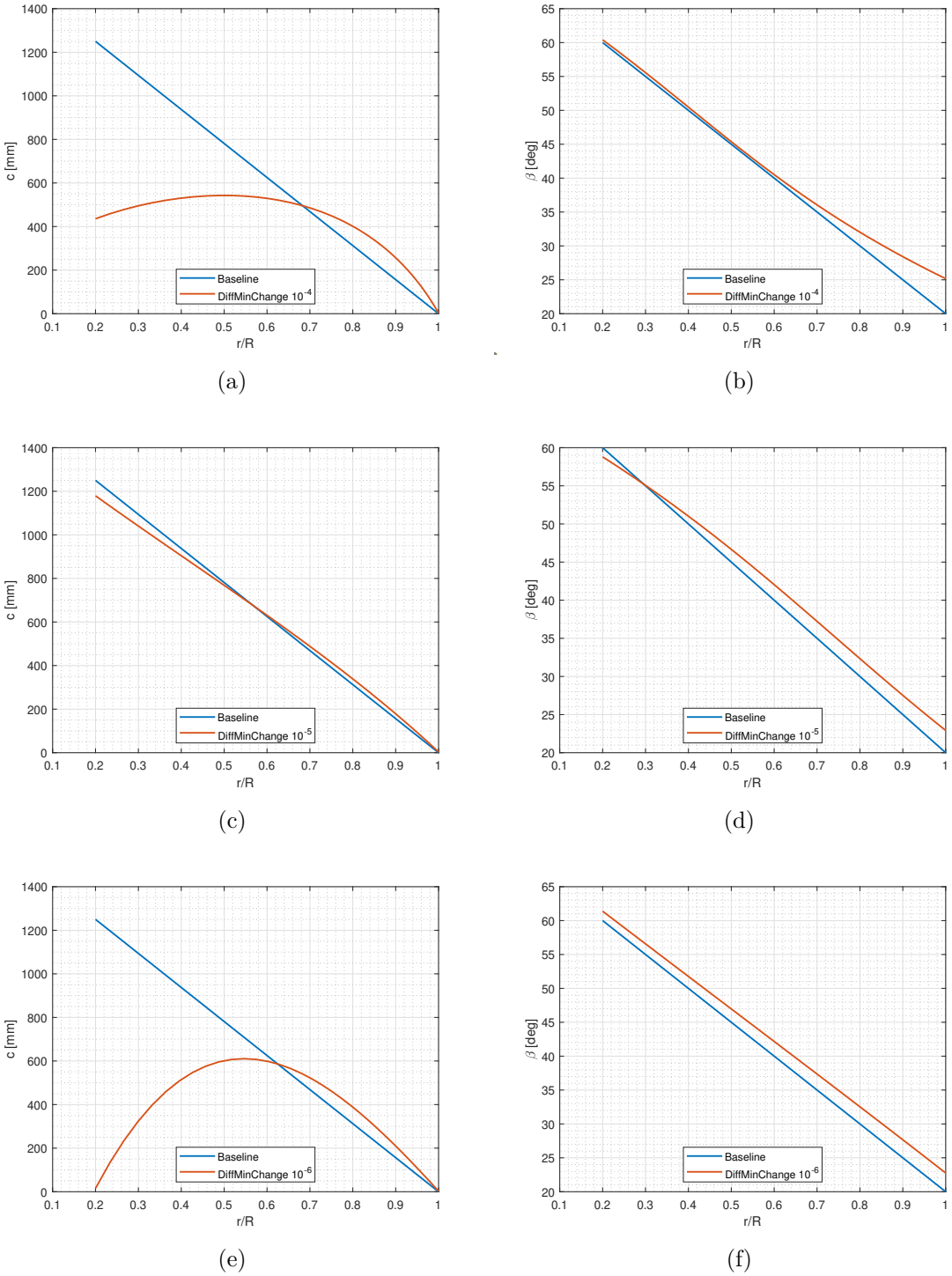

Figure B.6: Optimal geometries. Second initial guess - 2 (3)

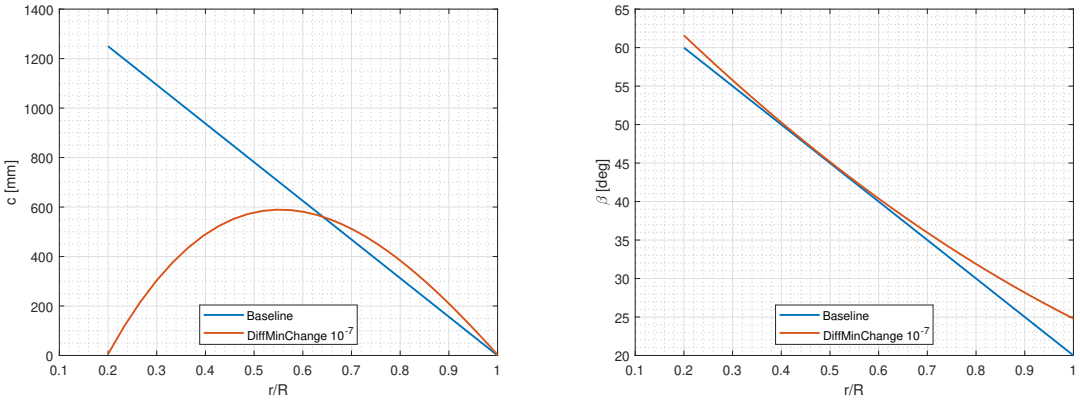

(a) (b)

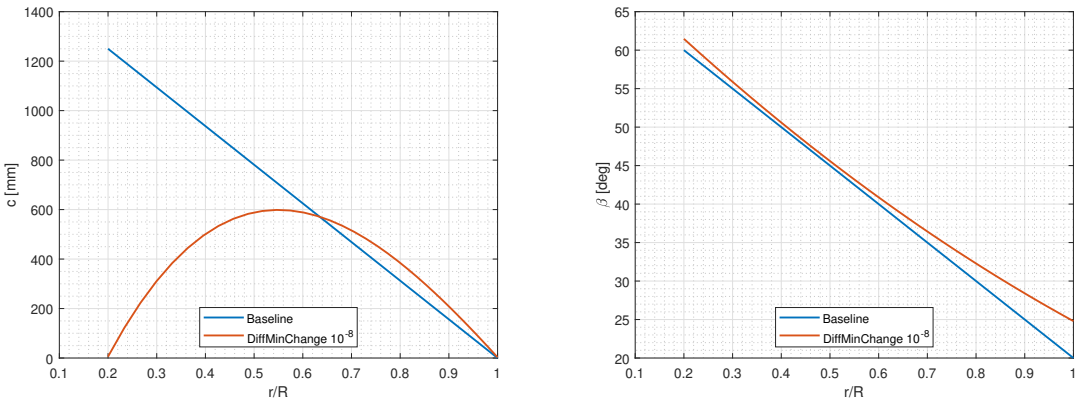

(c) (d)

Figure B.7: Optimal geometries. Second initial guess - 3 (3)